VILNIUS UNIVERSITY

Raimundas Sereika

INVESTIGATION OF ELECTRONIC STRUCTURE, OPTICAL AND DYNAMICAL PROPERTIES OF $A^{V}B^{VI}C^{VII}$ TYPE COMPOUNDS

Summary of doctoral dissertation

Physical sciences, physics (02 P)

Vilnius, 2013

The doctoral dissertation was prepared at Lithuanian University of Educational Sciences (Vilnius Pedagogical University) in 2008 – 2012.

Scientific supervisor:

Prof. Dr. Habil. Algirdas Audzijonis (Lithuanian University of Educational Sciences, physical sciences, physics – 02P)

The dissertation is being defended at the Physics Scientific Council at Vilnius University:

Chairman – Prof. Dr. Habil. Saulius Balevičius (State Scientific Research Institute Center of Physical Sciences and Technology, physical sciences, physics – 02P).

Members:

Prof. Dr. Habil. Valdas Sirutkaitis (Vilnius University, physical sciences, physics – 02P);

Assoc. Prof. Dr. Robertas Grigalaitis (Vilnius University, physical sciences, physics – 02P);

Prof. Dr. Habil. Alfonsas Grigonis (Kaunas University of Technology, physical sciences, physics – 02P);

Prof. Dr. Habil. Eugenijus Šatkovskis (Vilnius Gediminas Technical University, physical sciences, physics – 02P).

Opponents:

Prof. Dr. Nerija Žurauskienė (State Scientific Research Institute Center of Physical Sciences and Technology, physical sciences, physics – 02P);

Prof. Dr. Antanas Kiveris (Lithuanian University of Educational Sciences, physical sciences, physics – 02P).

The dissertation will be defended under open consideration in the Council of Scientific Field of Physics at 2 p. m. on January 8, 2013 at the Faculty of Physics and Technology of Lithuanian University of Educational Sciences, room 304.

Address: Studentu st. 39, LT-08106, Vilnius, Lithuania.

The summary of doctoral dissertation has been distributed on the 16th of November, 2012. The doctoral dissertation is available for review at the libraries of the Lithuanian University of Educational Sciences and Vilnius University.

VILNIAUS UNIVERSITETAS

Raimundas Sereika

$A^{V}B^{VI}C^{VII}$ TIPO JUNGINIŲ ELEKTRONINĖS STRUKTŪROS, OPTINIŲ IR DINAMINIŲ SAVYBIŲ TYRIMAS

Daktaro disertacijos santrauka

Fiziniai mokslai, fizika (02 P)

Vilnius, 2013

Disertacija rengta 2008 – 2012 metais Lietuvos edukologijos universitete (Vilniaus pedagoginiame universitete).

Mokslinis vadovas:

Prof. habil. dr. Algirdas Audzijonis (Lietuvos edukologijos universitetas, fiziniai mokslai, fizika – 02P)

Disertacija ginama Vilniaus universiteto Fizikos mokslo krypties taryboje:

Pirmininkas – Prof. habil. dr. Saulius Balevičius (Valstybinis mokslinių tyrimų institutas Fizinių ir technologinių mokslų centras, fiziniai mokslai, fizika – 02P).

Nariai:

Prof. habil. dr. Valdas Sirutkaitis (Vilniaus universitetas, fiziniai mokslai, fizika – 02P);

Doc. dr. Robertas Grigalaitis (Vilniaus universitetas, fiziniai mokslai, fizika – 02P);

Prof. habil. dr. Alfonsas Grigonis (Kauno technologijos universitetas, fiziniai mokslai, fizika – 02P);

Prof. habil. dr. Eugenijus Šatkovskis (Vilniaus Gedimino technikos universitetas, fiziniai mokslai, fizika – 02P).

Oponentai:

Prof. dr. Nerija Žurauskienė (Valstybinis mokslinių tyrimų institutas Fizinių ir technologinių mokslų centras, fiziniai mokslai, fizika – 02P);

Prof. dr. Antanas Kiveris (Lietuvos edukologijos universitetas, fiziniai mokslai, fizika – 02P).

Disertacija bus ginama viešame Fizikos mokslo krypties tarybos posėdyje 2013 m. sausio 8 d. 14 val. Lietuvos edukologijos universiteto, Fizikos ir technologijos fakulteto 304 auditorijoje.

Adresas: Studentų g. 39, LT-08106, Vilnius, Lietuva.

Disertacijos santrauka išsiuntinėta 2012 m. lapkričio 16 d.

Disertaciją galima peržiūrėti Lietuvos edukologijos universiteto ir Vilniaus universiteto bibliotekose.

TABLE OF CONTENTS

Structure of the dissertation

The dissertation has been written in Lithuanian. It consists of approbation of the results, introduction (scientific novelty and practical value, the aims of the work, the tasks of the work and defended propositions), 8 chapters (first two are literature review and research methodology, the remaining part describes and analyzes the results of the work), conclusions, references and appendix. In total, there are 108 typewritten pages containing 9 tables and 47 figures.

INTRODUCTION

The $A^{V}B^{VI}C^{VII}$ (were A^{V} – As, Sb, Bi; B^{VI} – O, S, Se, Te; C^{VII} – F, Cl, Br, I) compounds are semiconductors – ferroelectrics. It is well known that some of them posses phase transitions. These compounds are mostly characterized by a high piezomodulus, extensive sensitivity to the external pressure, complicated anisotropic structure, high photo conductivity and very strong forbidden gap dependence on the temperature. They host pyroelectric, electro-mechanical, electro-optical and many other nonlinear optical effects. Technologically, these compounds easily adapted to the low-pressure sensors, microwave, and piezoelectric devices [1-3], and are also used as memory elements [5-7].

Among these ternary compounds the most popular and the best studied is the SbSI crystal. In 1962, it was discovered that SbSI crystal has a ferroelectric phase transition, its temperature is $T_c \approx 295$ K [1-3]. Therefore, this compound had a large experimental physics community focus. SbSBr crystal also has a ferroelectric phase transition at a temperature $T_c = 22.8$ K [1, 2]. The low temperature phase transition has been far less studied experimentally. However, both of these compounds attracted the attention of theorists. In 1968, the trictritical point was detected [4]. A multitude soft-mode researches were performed. The anomalies near the ferroelectric phase transition region were investigated. For the crystal growth a number of methods were tested. The simplest of these – directly connecting the primary elements. SbSI can be easily obtained by fusion of Sb_2S_3 and SbI_3 and then cooled alloy treated with diluted hydrochloric acid, or by heating iodine with antimony sulfide Sb_2S_3. However, development of modern technologies increasingly popular in nanotechnology, proposed new production

techniques, allowing compounds to get smaller and larger technological perspectives. In 1999, SbSI quantum dots synthesized in the Na_2O-B_2O_3-SiO_2 organic modified silicates matrix by the sol-gel technique [8]. After that, SbSI nanocrystals were produced in organically modified TiO_2 glass [9, 10]. Later, SbSI nanorods were prepared by hydrothermal [11], ball milling [12], as well as ultrasound irradiation [13, 14] methods.

Lately among the compounds with bismuth atoms, lately, many industrial prospects of the development of electronic devices [15], energy-saving and solar cell production [16-19], even in applications in wastewater treatment plants [20-21] were discovered. In addition to the practical application these compounds are interesting for the fundamental research. Most of the published experimental data comes without physical phenomena interpretation. The analyzing of the experimental results and searching for solutions have a principled theoretical value, which determines the electronic structure of the compounds. As it is known, the benefit of fundamental research shows well after, but their scope is much broader, and gives major effect. These investigations lead to the progress of society. Therefore, it is important to investigate and explain these compounds occurring in the physical processes which determine the properties of the substance.

Scientific novelty and practical value

With the help of modern technology, for the first time, dependencies of the electronic structure, optical spectra, thermodynamic functions and so on were calculated in a wide range of energies. Calculations were compared with experimental measurements, as well as by other authors in similar calculations. In theory, the results explained the nature of the optical anomalies and phase transitions of the SbSBr and SbSI crystals. Investigations of the electronic structure and optical properties of these compounds have helped clarify the nature of the anisotropy, which, among other things, helps determine the electron density of states in valence band, inter-atomic electron charge distribution, and plasmon frequency of the movement.

For the first time in the field of experimental spectroscopic ellipsometry, our work has measured the vapor produced, SbSI, $SbSe_xS_{1-x}I$, BiSI, BiSeI, BiSBr, BiSeBr, and SbSeBr crystals. Single crystals grown using the Bridgman–Stockbarger method have

been studied at high temperatures and at various frequencies by measuring the electrical capacitance and resistance along the ***c(z)*** crystallographic axis. The newly discovered phenomenon [S17] shows the incomplete nature of investigations into these compounds and suggests reconsidering the published specifications. The work carried out theoretical and experimental studies providing further insight into the structure of $A^{V}B^{VI}C^{VII}$ compounds, and highlighting the most urgent and least explored areas.

The aims of the work

- To investigate the electronic structure and optical properties of the BiSI, BiSCl, BiSBr, BiSeI, BiSeBr, SbSI, SbSeI and SbSeBr semiconductor – ferroelectric compounds.
- To perform chemical bond investigation in the BiSBr and BiSeBr compounds.
- To investigate vibrational spectra and thermodynamic functions of the BiSI, BiSCl, SbSI and SbSBr compounds.
- To investigate SbSI and SbSeI crystals' permittivity changes in the 270 – 440 K temperature range.

The tasks of the work

1. To combine theoretical calculations searching for the optimal combination of the corresponding elementary unit cell parameters. To perform volume optimization calculations. Select the appropriate approximation for the calculations.
2. To calculate $A^{V}B^{VI}C^{VII}$ type compounds' electronic structure and optical spectra.
3. To measure and describe the SbSI and SbSeI crystals' permittivity changes in antiferroelectric phase transition area.
4. To calculate inter-atomic electron charge density distribution in BiSBr and BiSeBr crystals. To evaluate the covalent and ionic factors in the inter-atomic bonds.
5. To verify and approve theoretically experimental SbSI birefringence at the ferroelectric phase transition region.
6. To calculate $A^{V}B^{VI}C^{VII}$ type compounds' phonon density of states, dispersion and thermodynamic functions in harmonic and quasiharmonic approximations.

7. To find the difference between the thermodynamic functions in harmonic and quasiharmonic approximations in SbSI, SbSBr crystals' ferroelectric and paraelectric phases.
8. To identify interacting and not interacting phonon influence on the ferroelectric phase transition of SbSI and SbSBr crystals.

Defended propositions

1. $A^{V}B^{VI}C^{VII}$ type crystals' valence and conduction bands are composed of individual atoms' p and s orbital's. Electron density of states and electronic band configuration of the structure is determined by the electronic band transitions, as well as different charges and bond strength between atoms in surface and volume layers.
2. Optical functions spectra of $A^{V}B^{VI}C^{VII}$ type crystals have a strong anisotropy, and maximums are affected by interband optical transitions.
3. SbSI crystal birefringence in the ferroelectric phase depends on the spontaneous polarization.
4. Elementary unit cell parameters and phonon-phonon interaction are the substantial subjects of ferroelectric phase transition appearance in SbSI and SbSBr crystals.
5. The strong phononic interaction and lattice parameters determine strong B_{1u} soft mode anharmonic behavior and create double-well electronic potential, depending on the temperature.

1 LITERATURE REVIEW

This chapter presents the review of scientific literature on $A^{V}B^{VI}C^{VII}$ type compounds at work used theory and its specificity. The individual subsections explicate the main details about the structure of these materials, describes the most and least explored areas. It also portrays discovered and investigated effects of these compounds, their causes and nature. Below is a brief description of the main chapter highlights.

1.1 $A^{V}B^{VI}C^{VII}$ type crystal structure and chronology of research

This thesis analyzes $A^{V}B^{VI}C^{VII}$ type crystals consisting of chains extended in ***c(z)***-axis direction. Elementary cell contains four atoms of each type (Fig. 1. presents SbSI crystal lattice image in paraelectric phase). The atoms inside the chains are bind by covalently strong – ionic relations, and between neighboring chains weak Van der Waals forces operate. Therefore, crystal growth rate along the chains is 50 times greater than the perpendicular direction. Grown from the vapor phase usually grow crystals of needle shape, whose axis coincides with the crystallographic ***c(z)***-axis. These crystals' cross-sectional shape is not strictly defined and the area is small. The dimensions of the single crystal are approximately $2 \times 2 \times 15$ mm^3.

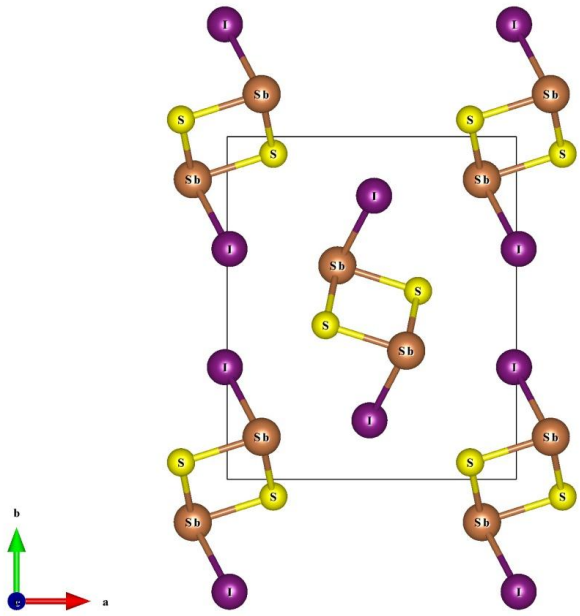

Fig. 1. The elementary unit cell of SbSI crystal in ***a(x)-b(y)*** plane. For the drawing atomic radius were used.

In 1950, the crystal lattice structure of SbSI was established by Dönges [22]. Accuracy of the test was not great, however was then followed by many studies, which made it possible to determine the exact $A^{V}B^{VI}C^{VII}$ type crystals lattice parameters and coordinates. Most of these crystals crystallize in paraelectric phase, 62nd orthorhombic space group $Pnam$ (D_{2h}^{16}). The location of the equivalent atoms in the elementary cell can be determined from Wyckoff spatial coordinates of the group:

$$x, y, \frac{1}{4};\ \bar{x}, \bar{y}, \frac{3}{4};\ \frac{1}{2} - x, \frac{1}{2} + y, \frac{3}{4};\ \frac{1}{2} + x, \frac{1}{2} - y, \frac{1}{4}.$$

However, not all $A^{V}B^{VI}C^{VII}$ compounds crystallize in $Pnam$ (D_{2h}^{16}) space group. For example, the BiOCl, BiOBr and BiOI crystals crystallize in tetragonal $P4/nmm$ (D_{4h}^{7}) space group. BiTeBr and BiTeI crystals are forming in the hexagonal $P\bar{3}m1$ (D_{3d}^{3}) space group.

It is worth mentioning that among the $A^{V}B^{VI}C^{VII}$ compounds are popular and their mixtures research: $SbSe_xS_{1-x}I$, $SbSBr_xI_{1-x}$, $Bi_xSb_{1-x}SI$, $SbO_xS_{1-x}I$, $As_xSb_{1-x}SI$, as the transition temperature depends on the composition of the mixture. It is known, that $SbSe_xS_{1-x}I$ transition temperature T_c = 0 – 298 K, $SbSBr_xI_{1-x}$ crystal phase transition temperature T_c = 22.8 – 298 K, where x varies from 1 to 0.

The literature describes various ways to modify $A^{V}B^{VI}C^{VII}$ type compounds [23-27]. The aim is to investigate the effects of impurities in crystals to enhance effects that raise or lower the phase transition temperature, and so on. The authors [25] found that the SbSI crystals with a specific, additional Sb_2S_3 matter raises the ferroelectric phase transition temperature to 314 K. The phase transition temperature also changes if the SbSI crystal growth during the introduction of a Cl content [26]. Variously modified SbSI crystals were also explored by the other authors for the different purposes.

1.2 Density Functional Theory and its equipment

The solids consist of heavy, positively charged particles (nuclei) and lighter, negatively charged particles (electrons). If you have a system of N nuclei, we are dealing with N + ZN each other electromagnetically interacting particle problem. This is called the

"many-body" problem and it is solved by using quantum mechanics. The exact "many-particle" hamiltonian for this system is:

$$\hat{H} = -\frac{\hbar^2}{2}\sum_i \frac{\nabla^2_{\vec{R}_i}}{M_i} - \frac{\hbar^2}{2}\sum_i \frac{\nabla^2_{\vec{r}_i}}{m_e} - \frac{1}{4\pi\varepsilon_0}\sum_{i,j}\frac{e^2 Z_i}{\left|\vec{R}_i - \vec{r}_j\right|} + \frac{1}{8\pi\varepsilon_0}\sum_{i\neq j}\frac{e^2}{\left|\vec{r}_i - \vec{r}_j\right|} + \frac{1}{8\pi\varepsilon_0}\sum_{i\neq j}\frac{e^2 Z_i Z_j}{\left|\vec{R}_i - \vec{R}_j\right|}. \qquad (1.1)$$

Here M_i – mass of the nucleus, Z_i – charge of the nucleus and $\vec{R}_i$ is its position vector. The mass and position of the electron are m_e and $\vec{r}_i$, respectively. The first part of this hamiltonian describes the nuclei kinetic energy operator. Second – electron kinetic energy operator. The remaining three parts of the hamiltonian describe the Coulomb interaction between electrons and nuclei, between electrons and other electrons, and between nuclei and other nuclei.

It is out of question to solve this problem exactly and almost impossible [28]. For such systems a wide array of additional approximations are needed. In the literature, two main methods are known: Hartree-Fock method (used mainly in theoretical chemistry calculations) and Density Functional Theory (DFT). The latter method is used mainly in theoretical physics calculations [28, 29]. The calculations are carried out with a self-consistent scheme by solving the Kohn-Sham equations. In the dissertation, a detailed description of the DFT equations is given, as well as used approximations. However, in summary it should be noted that author mainly used the Full Potential Linearized Augmented Plane Wave (FP-LAPW) method [29] in the frame work of DFT along with Generalized Gradient Approximation (GGA) [30].

2 RESEARCH METHODOLOGIES

2.1 Experimental research methodology

For the experimental investigations SbSI, SbSeI, $SbSe_xS_{1-x}I$, $SbSI(Sb_2S_3)_x$, BiSI, BiSeI, BiSBr, BiSeBr and SbSeBr crystals were grown from the vapor phase and using the Bridgman-Stockbarger method.

2.1.1 Optical experimental research

This work uses the rotating analyzer method [31, 32]. In this case, the light intensity is scanning full analyzer turn - 360°. Simplest way electric vector-ray incidence plane angle is 45°. Then the intensity *I* of the polarized light beam after reflection at the sample is modulated by the rotating analyzer according to:

$$I = \frac{I_0}{2}\left(1 - \cos 2\Psi \cos 2\alpha + \sin 2\Psi \cos \Delta \sin 2\alpha\right), \tag{2.1}$$

where α is the angular position of the analyzer, I_0 – incident light intensity of the sample and Ψ, Δ are geometry depended ellipsometric parameters which connect to the dielectric properties of the surface measured [33]:

$$\varepsilon_{re} = n^2 - k^2 = \sin\varphi\left[1 + \tan^2\varphi \frac{\cos^2 2\Psi - \sin^2 2\Psi \sin^2}{\left(1 - \sin 2\Psi \cos\Delta\right)^2}\right] \tag{2.2}$$

$$\varepsilon_{im} = 2nk = \sin^2\varphi \tan^2\varphi \frac{\sin 2\Psi \cos 2\Psi \cos 2\psi}{\left(1 - \sin 2\psi \cos\Delta\right)^2} \tag{2.3}$$

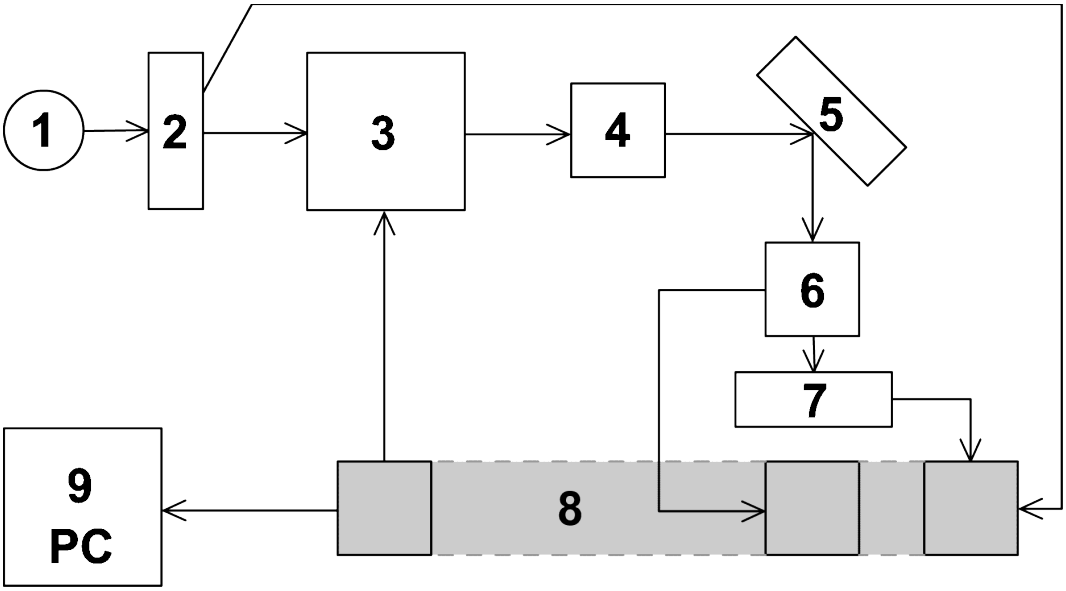

Fig. 2. A block diagram of the optical configuration system: 1 – light source, 2 – light intensity modulator, 3 – pc controlled monochromator, 4 – polarizer, 5 – sample, 6 – pc controlled analyzer, 7 – light intensity detector, 8 – amplifier block system, 9 – personal computer.

Investigation was performed at the temperature 295 K using spectrum ellipsometer, which can measure energy in the range of 0.5 – 5.0 eV (incident angle 70°). A block diagram of the optical configuration system is shown in Fig. 2.

For analysis, first the light intensity of known wavelength and the analyzer angle α is measured. Then ellipsometric parameters values Ψ and Δ are found. Lastly crystal dielectric constants ε_{re}, ε_{im} and optical constants n, k are calculated. Investigative crystals were with crystallographic ***c***-axis which was in the reflection plane. Therefore the measurements are performed in both perpendicular and parallel positions of the incidence plane.

2.1.2 Dielectric and electric research

These studies have been performed using crystals grown by Bridgman-Stockbarger method. It is therefore comfortable to carry out measurements along the ***c***-axis. Crystals grow in the hermetic vacuum ampoules with a length of about 15 cm and cross-sectional area of about 1 cm^2. Grown crystals were cut with a diamond saw into approximately 4 mm thick tablets and then polished.

Crystal dielectric and electrical properties were measured with a "GW Instek LCR-819" device. The crystals with the thermocouple were placed in the furnace, where the sample was trapped with the contacts on both sides for about 1 cm^2 area. The electrical capacitance and resistance were measured at various fixed frequencies (from 50 Hz to 100 kHz) by changing the temperature of the system.

2.2 Theoretical calculation methodology

Modern theoretical physics calculations are essentially based on computer modeling and calculations with extremely fast computers using quantum physics. In this way it is possible to fulfill very difficult researches and investigations in broad areas of energy, etc. LAPW method is one of the most accurate and reliable methods for the solid-state calculations, exploring the electronic structure of materials, and so on. [28, 29]. Currently, DFT and LAPW research is quite widely used in various combinations. For this purpose a number of computer programs are written (WIEN2k, VASP, FHI-AIMS,

CASTEP, abinit, SIESTA, Quantum ESPRESSO, OCTOPUS, etc.). In this work computer program Wien2k [29] and for the crystals lattice dynamics studies – PHONON [34] are used.

2.2.1 A computer program WIEN2k

The program package uses DFT with the FP-LAPW (Full Potential Linearized Augmented Plane Wave) method. The program is written in a Fortran language and adapted to the Linux operating system. Consequently the Fortran compiler and the relative libraries are needed in the system. Our calculations were performed on a Red Hat Enterprise Linux 6 operating system with the Intel Fortran Compiler v11.0. Also we used some helpful utilities such us emacs, ghostscript, gnuplot, XcrySDen and so.

Wien2k can be used for investigations of the electron density of states, band structure, optical properties of compounds such as dielectric permittivity, refractive indices, etc. For the basic calculations the main compound characterizing information is needed: Equivalent atom positions in the elementary cell, lattice parameters, space group and atomic radiuses (RMT). With these data and having sufficient size *k*-mesh the electron density of states in the material can be calculated.

Dielectric functions $\varepsilon_1(\omega)$ and $\varepsilon_2(\omega)$, refractive index $n(\omega)$, extinction $k(\omega)$, electron energy loss function $L(\omega)$, absorption $K(\omega)$, reflectivity $R(\omega)$ coefficients and optical conductivity $\sigma(\omega)$ spectra are calculated from these equations:

$$\varepsilon_1(\omega) = 1 + \frac{2}{\pi} P \int_0^{\infty} \frac{\varepsilon_2(\omega')\omega'}{\omega'^2 - \omega^2} d\omega', \tag{2.4}$$

$$\varepsilon_2(\omega) = \frac{Ve^2}{2\pi\hbar m^2 \omega^2} \int d^3k \sum_{n,n'} \left| \left\langle \vec{k}n \middle| \vec{p} \middle| \vec{k}n' \right\rangle \right|^2 f(\vec{k}n) \cdot \left[1 - f(\vec{k}n')\right] \delta(E_{\vec{k}n} - E_{\vec{k}nn'} - \hbar\omega), \tag{2.5}$$

where $\hbar\omega$ is the photon energy, V – volume, P – Cauchy's principal value of an integral, $\vec{p}$ – momentum operator, $\left|\vec{k}n\right\rangle$ – crystal wave function, $E_{\vec{k}n}$ – the energy of the electron in the n^{th} state and $f(\vec{k}n)$ – Fermi distribution.

$$n(\omega) = \frac{1}{\sqrt{2}}\left[\sqrt{\varepsilon_1^2(\omega) + \varepsilon_2^2(\omega)} + \varepsilon_1(\omega)\right]^{\frac{1}{2}}, \tag{2.6}$$

$$k(\omega) = \frac{1}{\sqrt{2}}\left[\sqrt{\varepsilon_1^2(\omega) + \varepsilon_2^2(\omega)} - \varepsilon_1(\omega)\right]^{\frac{1}{2}}, \tag{2.7}$$

$$L(\omega) = -\mathrm{Im}\left(\frac{1}{\varepsilon}\right) = \frac{\varepsilon_2(\omega)}{\varepsilon_1^2(\omega) + \varepsilon_2^2(\omega)}, \tag{2.8}$$

$$K(\omega) = \frac{2\omega}{c}k(\omega), \tag{2.9}$$

$$R(\omega) = \left|\frac{\tilde{n} - 1}{\tilde{n} + 1}\right| = \frac{(n-1)^2 + k^2}{(n+1)^2 + k^2}, \tag{2.10}$$

$$\mathrm{Re}\,\sigma(\omega) = \frac{\omega}{4\pi}\varepsilon_2(\omega). \tag{2.11}$$

The program first calculates $\varepsilon_1(\omega)$ and $\varepsilon_2(\omega)$. Then using (2.6) – (2.11) equations are calculated $n(\omega)$, $k(\omega)$, $L(\omega)$, $K(\omega)$, $R(\omega)$, $\mathrm{Re}\,\sigma(\omega)$ and $\mathrm{Im}\,\sigma(\omega)$. The complex dielectric constant of a solid $\varepsilon(\omega)$ has a following form: $\varepsilon(\omega) = \varepsilon_1(\omega) + i\varepsilon_2(\omega)$.

In this work we have used $A^{V}B^{VI}C^{VII}$ crystals' atomic coordinates and lattice parameters, which are given in the annex of the dissertation. There is also a list of the atomic radii used for calculations. Electronic structure and optical properties were studied with a mesh of 5000 *k*-points in the irreducible part of the Brillouin zone. Lattice vibrations and thermodynamic functions were studied with a mesh of 100 *k*-points in the irreducible part of the Brillouin zone. The calculations were performed with a plane wave cut-off $k_{\max} = 7/R^{MT}$ (Here R^{MT} is the radius of the smallest muffin-tin sphere). The iteration halted when the difference in the eigen values was less than 0.0001 between steps of convergence criterion. The separation of valence and core states was chosen as -6.0 Ry.

2.2.2 Lattice dynamics studies with PHONON

Temperature of solids is almost entirely determined by phonons. Phonons, in turn, are defined as a combination of atomic vibrations. Phonons are responsible for thermal

expansion; they contribute to appearance of phase transitions, and phase diagrams. Phonons also play a role in elastic and dielectric constants, transport processes, such as diffusion and chemical reactions, superconductivity, ferroelectricity, shape memory alloys, etc. Fairly qualitative all these things and much more can be explored with a PHONON [34] software. As an input this software requires to know crystal structure and Hellmann-Feynman forces. External *ab initio* program like Wien2k, VASP, MedeA of Materials Design, or Siesta can be used in this respect. Such a way is possible to get the dispersion curves, phonon density of states, thermodynamical functions, neutron and x-rays spectroscopic spectra, and many others quantities.

3 CHEMICAL BONDING ANALYSIS

The character of the chemical bond leads to the electron charge density distribution in the inter-atomic bonds. In order to evaluate the covalent and ionic factor assessment we have performed electron charge density distribution calculations. For this task BiSBr and BiSeBr crystals were chosen. The authors of Ref. [35] have studied charge density of BiSeBr crystal. They have used the pseudopotential method and found that the bonding between Bi and Se is more covalent than the bonding between Bi and Br. Physically, after the electrons are transferred to the Br ion, the Bi atom cannot provide enough charge to the Se to form an ionic bond. So, the Bi and Se compromise and form a covalent bond. We describe this composite feature as “ionic-covalent” bond. BiSeI crystal has a very similar feature. Bi-Se and Bi-I has the ionic-covalent bond. There is no connection at all between Se and I at all. The maximum charge density around Br is larger than that around I because Br is more electronegative than I. These charges are, for the most part, transferred from the metallic ion. Finally, the authors conclude that Bi in BiSeBr has less charge to form the covalent Bi-Se bond than it has in the BiSeI case.

Electron charge density distribution of BiSBr and BiSeBr was calculated using the atomic coordinates and lattice parameters taken from [36] literary source. Calculations were made between atoms: Bi-S, Bi-Se and Bi-Br. Figures 3-8 show the electron charge density distribution in various cases.

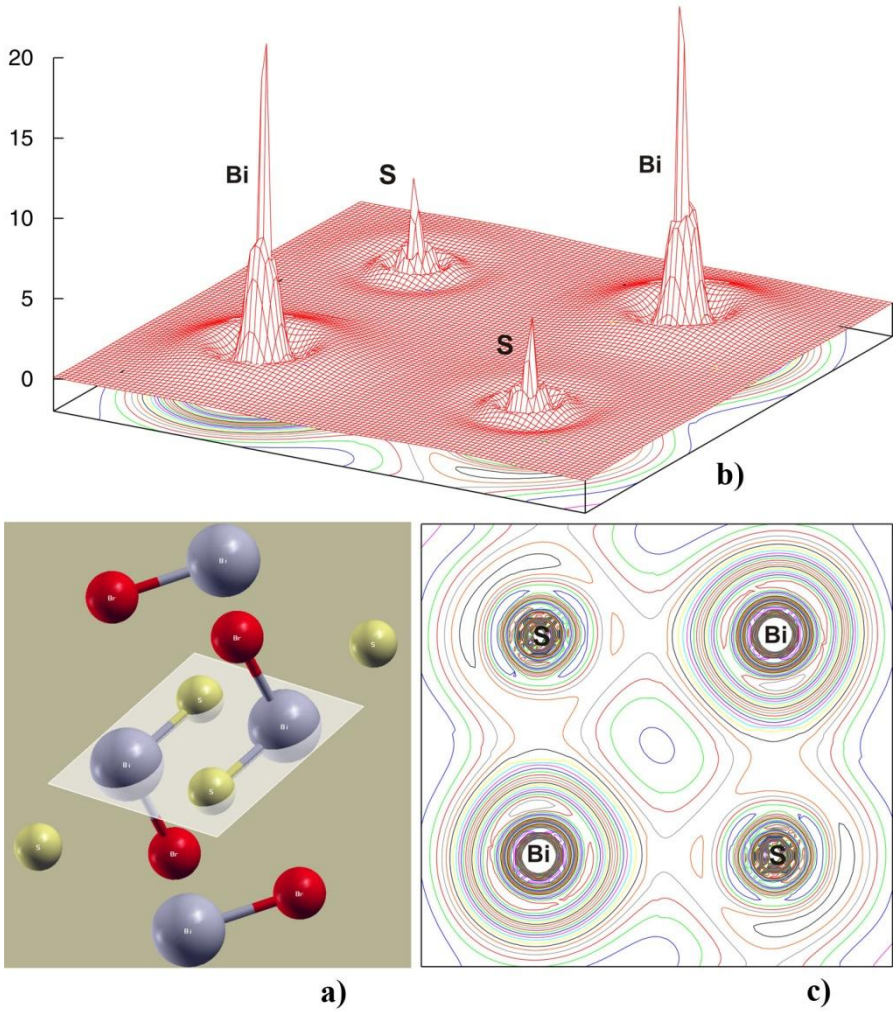

Fig. 3. a) Separated Bi(3), S(3), Bi(4) and S(4) atoms for displaying electron charge density: b) in space and c) in plane.

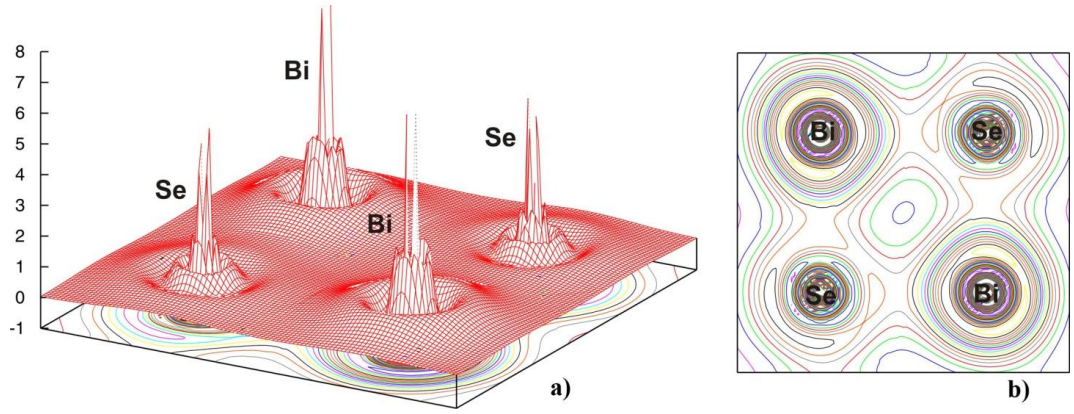

Fig. 4. The electron charge density for Bi(3), Se(3), Bi(4) and Se(4) atoms: a) in space, b) in plane.

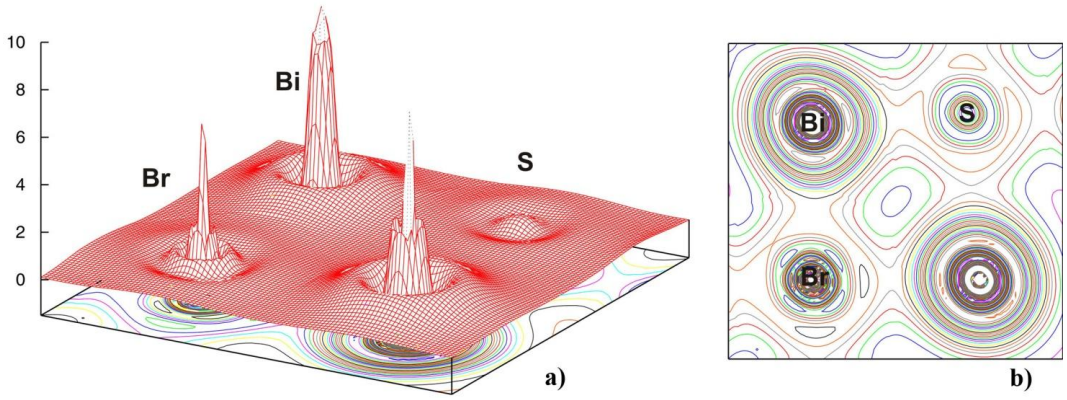

Fig. 5. The Bi(3), S(4), Br(1) molecule electron charge density: a) in space, b) in plane.

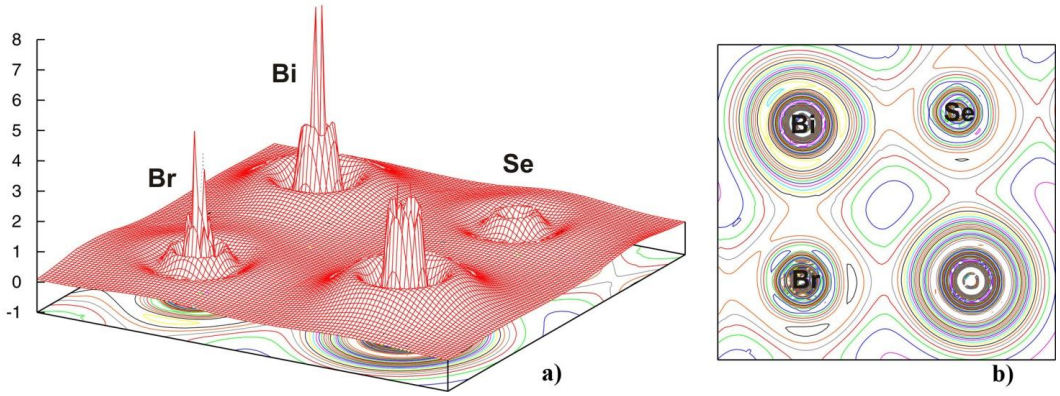

Fig. 6. The Bi(3), Se(3), Br(1) molecule electron charge density: a) in space, b) in plane.

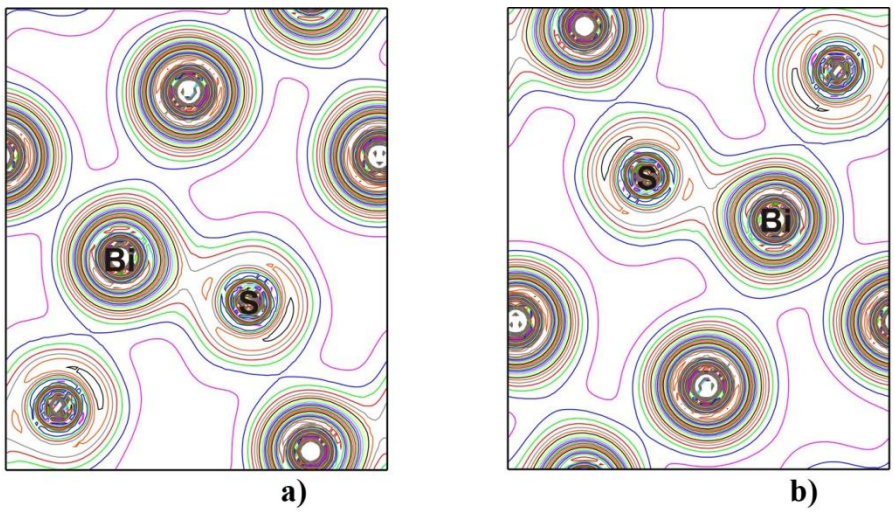

Fig. 7. BiSBr crystal's electron charge density: a) Bi(4) and S(4) marked in the plane z = 1/4, b) Bi(3) and S(3) marked in the plane z = 3/4.

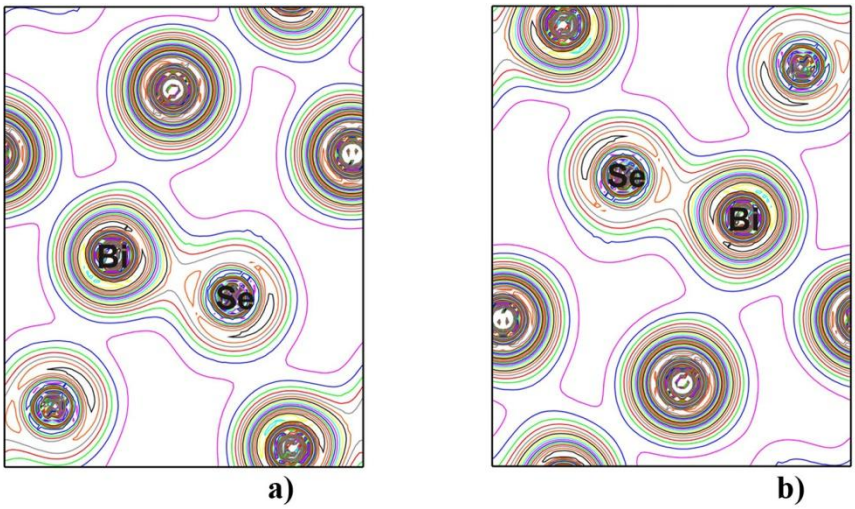

Fig. 8. BiSeBr crystal's electron charge density: a) Bi(4) and Se(4) marked in the plane z = 1/4, b) Bi(3) and Se(3) marked in the plane z = 3/4.

The obtained results indicate that the Bi-S and Bi-Se bondings have stronger covalent bonds than in Bi-Br, as between Bi and S (Bi and Se) distance is less than the distance between Bi and Br atoms. Considering the partial electron density of states (DOS) distribution the electron charge density distribution in the Bi, S and Br atomic bonds is caused by Bi – 6p, S – 3p, Se – 4p, Br – 4p orbital hybridization.

More accurate covalent connection strength can only be obtained by calculating inter-atomic bond ionicity factor f_i. Ionicity factor f_i can be calculated in different ways. One of the methods is to evaluate ionicity factor f_i using an empirical formula [37]:

$$f_i = \frac{1}{2}\left[1 - \cos\left(180° \frac{E_{AS}}{E_{VB}}\right)\right]. \qquad (3.1)$$

Here E_{AS} – distance (in electron-volts) between the two upper valence bands. E_{VB} – the total width of the all valence bands. E_{AS} and E_{VB} can be determined from the partial DOS distribution. For the BiSBr and BiSeBr crystals $E_{AS} = 3.3$ eV, $E_{AS} = 3.8$ eV and $E_{AS} = 5.0$ eV respectively for Bi-S, Bi-Se and Bi-Br bonding ($E_{VB} = 14.8$ eV). Thus, ionicity factor $f_i = 0.117$ for Bi-S, $f_i = 0.154$ for Bi-Se and $f_i = 0.255$ for Bi-Br bonds.

For the calculation of the ionicity factor by Pauling method [38], the folowing equation is used:

$$f_i^p = 1 - \exp\left[-\frac{(X_A - X_B)^2}{4} \right]. \quad (3.2)$$

Here X_A and X_B – electronegativity values for the corresponding atoms A and B. In our case electronegativity values for the Bi, S, Se and Br atoms are following: $X_{Bi} = 2.0$, $X_S = 2.5$, $X_{Se} = 2.4$ and $X_{Br} = 2.8$ [39]. Estimated ionicity factor by Pauling method $f_i^p = 0.060$ for Bi-S, $f_i^p = 0.039$ for Bi-Se and $f_i^p = 0.147$ for Bi-Br bonds.

4 ELECTRONIC STRUCTURE OF BiSI, BiSCl, BiSBr, BiSeI, BiSeBr, SbSI, SbSeI, SbSBr AND SbSeBr SEMICONDUCTOR AND FERROELECTRIC COMPOUNDS

4.1 Investigation of electron density of states

In solid-state and condensed matter physics, the density of states of a system describes the number of states per interval of energy at each energy level that are available to be occupied by electrons. Density of states can be compared with X-ray photoelectron emission spectra (XPS) of the valence band (VB) and the deep-level measurements. The theoretical photoelectron emission spectra of VB of BiSI crystal has been calculated from the partial DOS (Fig. 9) weighted with atomic photoemission cross-sections *s*(*i*, *l*):

$$total\text{-DOS} = \sum_i (s\text{-DOS})_i \, s(i,s) + \sum_i (p\text{-DOS})_i \, s(i,p), \quad (4.1)$$

where s-DOS, p-DOS – partial density of states of VB of *i*-atoms (Bi, S, I). To find photoemission cross-sections *s*(*i*, *s*) and *s*(*i*, *p*) from [40] we have used experimental X-ray photon energy 1486.6 eV (the X-ray photoemission spectra $A^VB^{VI}C^{VII}$ type crystals were obtained with monochromatic Al Kα radiation at room temperature using a spectrometer with energy resolution about 0.3 eV [41, 42]).

For comparison of the results total DOS of BiSI crystal weighted with *s*(*i*, *l*) and calculated using Wien2k [29] package is shown in Fig. 9. The experimental and

theoretical results of BiSI crystal are very similar. The differences for the most part are created by the thermal motion of atoms.

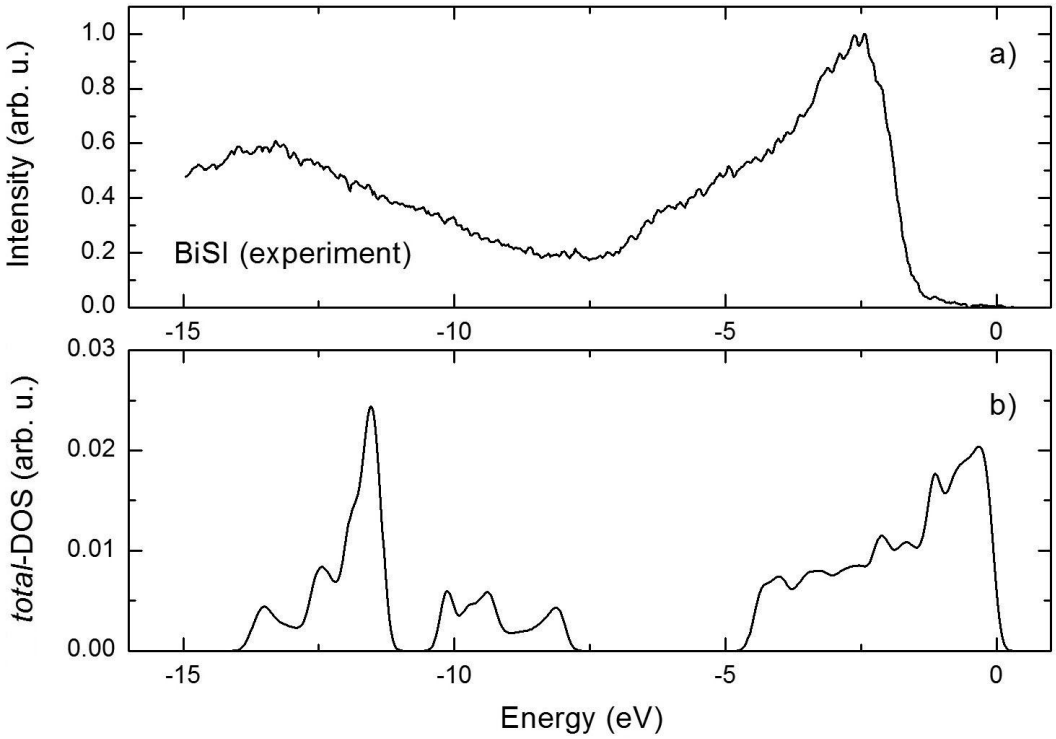

Fig. 9. a) Experimental XPS of BiSI crystal extracted from Ref. [42], b) *total*-DOS of BiSI crystal.

The SbSI crystal's DOS in valence band consists of three bands, which in turn are composed of hybridized Sb – 5p, Sb – 5s, S – 3p, S – 3s, I – 5s and I – 5p orbital (Fig. 10). Two lowest valence bands consist of Sb – 5s, S – 3s and I – 5s, while the higher valence band consists of Sb – 5p, S – 3p and I – 5p hybridized orbital. Conduction band up to 5 eV is composed of Sb – 5p, S – 3p and I – 5p hybridized orbital. SbSI DOS calculations are very similar to those which are given in [43, 44].

The DOS calculations for SbSeBr, BiSCl, BiSBr and BiSeBr crystals revealed that they have four valence bands. Their total and partial DOS distribution is very similar. Partial density of states maintain very similar s/p orbitals' domination for both valence and conduction bands.

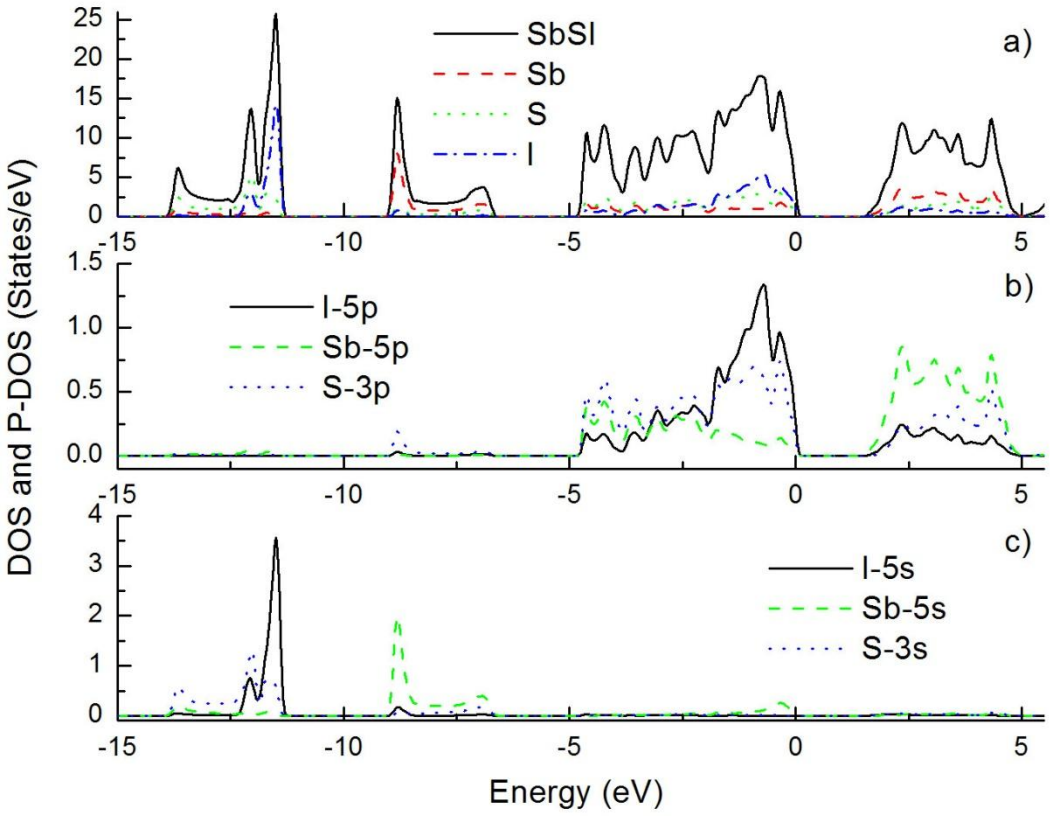

Fig. 10. The total and partial DOS of SbSI crystal. Calculated with atomic coordinates and lattice parameters taken from [45, 46] at 285 K temperature.

4.2 Investigation of electronic band structure

Electronic band structure was calculated through the main points of the first Brillouin zone (Fig. 11). The calculated band structures for BiSI and SbSeBr crystals are presented in Fig. 12. We have observed the presence of well-separated groups of bands. Our theoretical calculations reveal that BiSI and SbSeBr crystals have an indirect forbidden gap (the arrows denotes the location of indirect transition). For both crystals the minimum of the conduction band is located at Γ point and maximum of the valence band appears nearly midway between the Z and Γ points of the Brillouin zone (Fig. 12). The calculated value of the forbidden gap for BiSI crystal is 1.57 eV. These results confirm the experimentally determined BiSI band gap value, which is 1.59 eV [47]. The calculated value of the forbidden gap for SbSeBr crystal is 1.40 eV. These results are close to the experimental measurement results (when $\vec{E} \parallel \vec{c}$ E_g = 1.88 eV, when $\vec{E} \perp \vec{c}$ E_g = 1.92 eV) from Ref. [48]. Very large discrepancy in the band gap calculations was

obtained by the authors of Ref. [49]. They calculated the indirect transition band gap – 0.23 eV and the direct – 0.47 eV.

Other electronic band structure studies of $A^{V}B^{VI}C^{VII}$ compounds give very similar band lineup. Mostly bands come closely at Z and Γ points and depart at U and R points of the Brillouin zone.

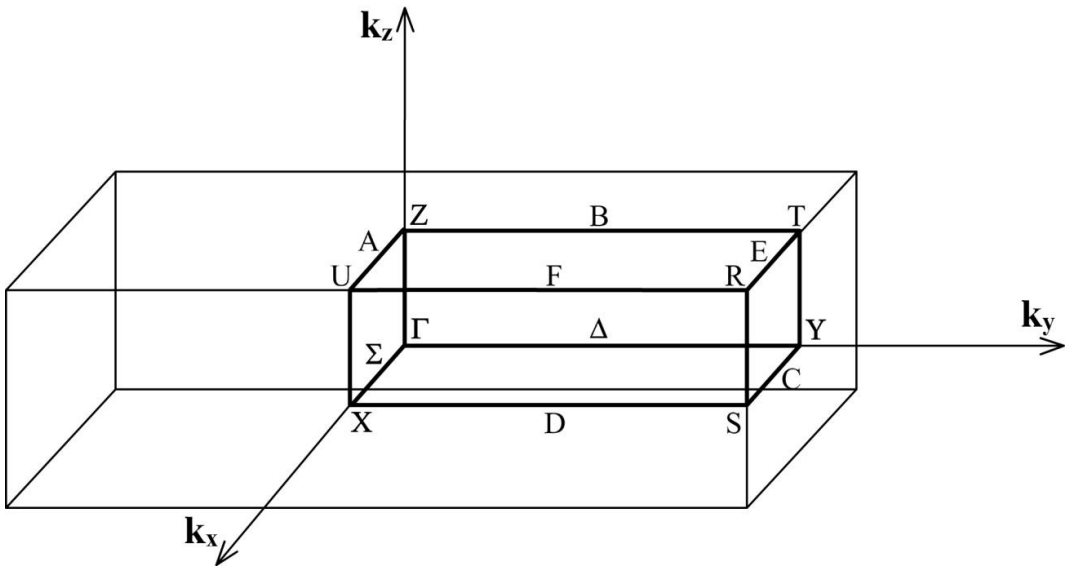

Fig. 11. The first Brillouin zone for the orthorhombic crystals.

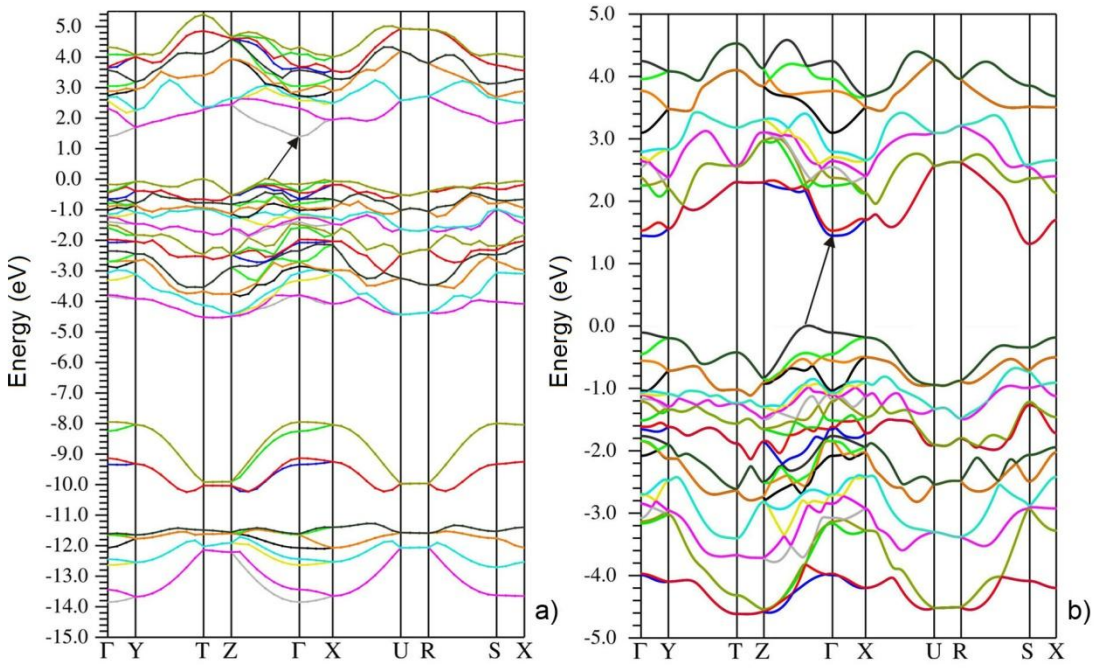

Fig. 12. a) Band structure of BiSI crystal, b) Band structure of SbSeBr crystal.

5 OPTICAL PROPERTIES OF BiSI, BiSCl, BiSBr, BiSeI, BiSeBr, SbSI, SbSeI, SbSBr AND SbSeBr SEMICONDUCTOR AND FERROELECTRIC COMPOUNDS

5.1 Investigation of the optical properties using spectroscopic ellipsometry technique

The optical properties of $A^{V}B^{VI}C^{VII}$ type compounds were studied by spectroscopic ellipsometry technique. Elipsometric measurements were performed at room temperature in the spectral range of 0.5 – 5.0 eV by means of a photometric ellipsometer with rotating analyzer [31, 32]. In the spectral range under consideration the ellipsometric parameters Ψ and Δ were measured with accuracy of 0.02°.

Experimental spectra of the dielectric functions were analyzed by contribution of Lorentzian type lines in the model of pseudo-dielectric function:

$$\varepsilon(E) = \sum_k \frac{A_k}{E_k^2 - E^2 - iE\Gamma_k}, \tag{5.1}$$

where A_k, E_k and Γ_k are amplitude, energy and k^{th} line width, respectively. The number of these parameters depends on oscillators used in physical model. We hold assumption that influence to the crystals' spectrum is from three or four oscillators. That influence depends on investigative crystal. The fitting parameters are obtained by minimization using the mean-square method of the difference between the calculated and experimental spectra of the dielectric constants' components approximately by Laurence lines with amplitude A_k, energy E_k and half-width Γ_k for samples.

We have found that for sufficient description of the $SbSe_xS_{1-x}I$ mixture spectra three oscillators are enough [S1]. BiSI, BiSeI, BiSBr and BiSeBr dielectric spectra with four Laurence oscillators are properly described [S4, S6, S12]. Fig. 13 shows that the total sums of the four oscillators contribute to the experimental spectra of dielectric functions for BiSeI crystals with an excellent agreement. The experiments were also compared with the DFT and the results are fully detailed in the dissertation.

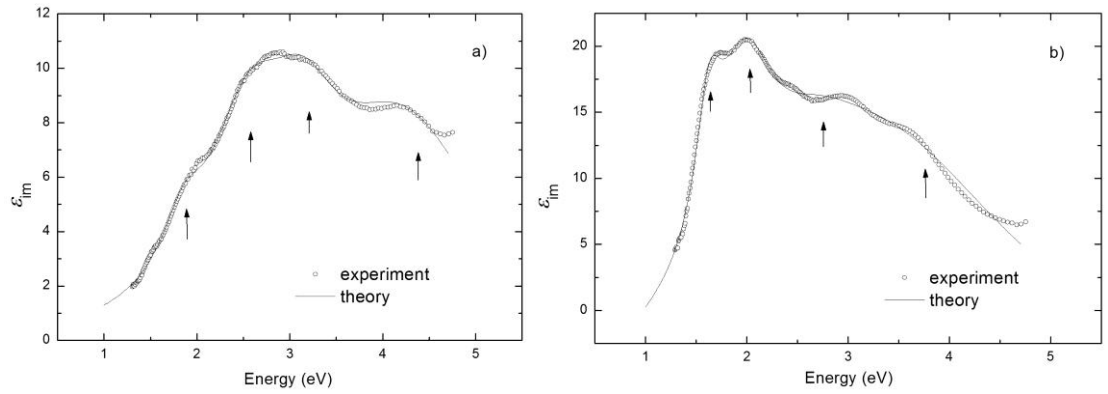

Fig. 13. Total oscillators' contribution (calculated by Eq. (5.1)) to the experimental ε_{im} spectra for the BiSeI crystal (arrows denotes positions of the Lorentz lines): a) when $\vec{E}\,||\,\vec{c}$ and b) when $\vec{E}\perp\vec{c}$.

5.2 Absorption, reflectivity and electron energy loss spectra

$A^{V}B^{VI}C^{VII}$ type crystals' spectra of each other are very similar. Absorption coefficient *K* dependence on photon energy, as well as the reflectance *R* dependence on photon energy in all three ***x***, ***y*** and ***z***-axis directions own two main large peaks, which in turn consists of smaller peaks (Figs. 14 and 15).

Fig. 14 shows the calculated reflectivity *R(E)* and absorption *K(E)* spectra of BiSI and BiSeI in two directions ***x*** znd ***z***. The first main reflection and absorption maximum for both crystals is in the 1 – 6 eV energy range. The second main reflection and absorption maximum for both crystals is approximately in the 6 – 20 eV energy range. The two main maxima are created by the interband electron transitions. These maxima and high anisotropic behavior are repeated for all $A^{V}B^{VI}C^{VII}$ orthorhombic structure crystals. The absorption edge normally takes place between the top of the valence band and the bottom of the conduction band.

At intermediate energies (0 – 30 eV) the energy losses are due to single electron excitations and collective excitations (plasmons). The energy of the maximum peak *L(E)* is assigned to the energy of volume plasmon peak $\hbar\omega_p$. At this energy, the real part of the dielectric function Re ε coming from the high frequency side goes through zero (vanishes). The maximum peak for BiSI crystal is located at the energy of 18 eV. Therefore, the value of volume plasmon energy is $\hbar\omega_p = 18\,\text{eV}$. The same plasmon

energy keeps in BiSeI and BiSeBr crystals. For the BiSCl crystal plasmon energy value is $\hbar\omega_p = 19\,\text{eV}$ and for BiSBr it is $\hbar\omega_p = 20\,\text{eV}$.

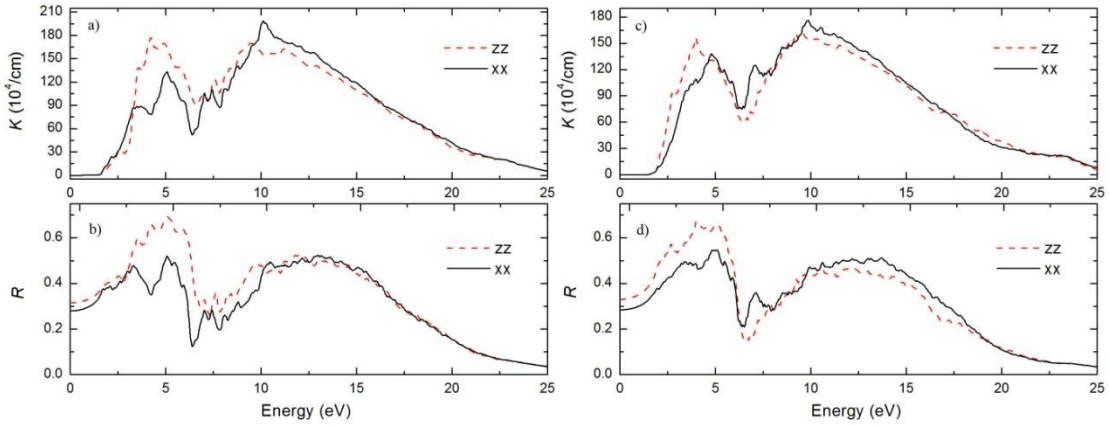

Fig. 14. The absorption spectra: a) for BiSI crystal, c) for BiSeI crystal.
The reflectivity spectra: b) for BiSI crystal, d) for BiSeI crystal.

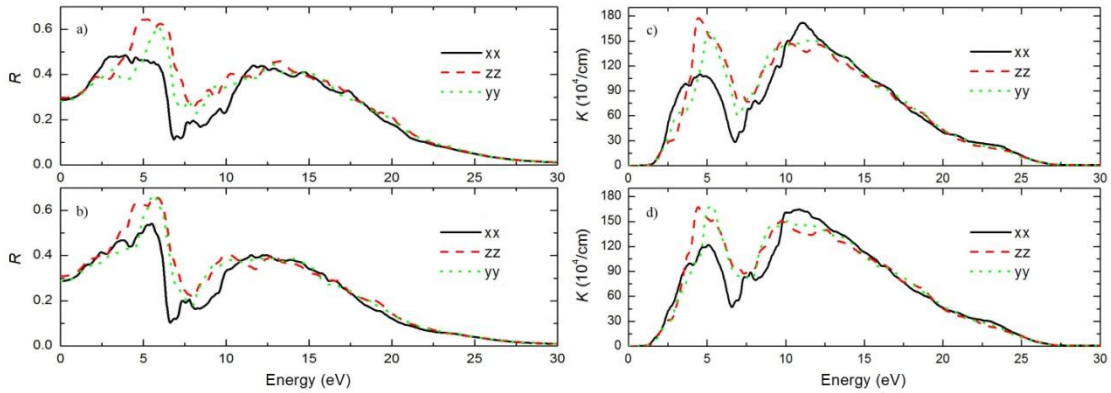

Fig. 15. The reflectivity spectra: a) for BiSBr crystal, b) for BiSeBr crystal.
The absorption spectra: c) for BiSBr crystal, d) for BiSeBr crystal.

For free electrons the plasmon energy is calculated according to the following model:

$$\hbar\omega_p = \hbar\sqrt{\frac{ne^2}{\varepsilon_0 m}}, \tag{5.2}$$

here n is the valence electron density, e is the elementary charge, m is the electron mass, ε_0 is the permittivity of free space, and $\hbar$ is the Planck constant.

The plasma frequency ω_p can also be tested with the sum rule [50]:

$$\frac{\pi}{2}\omega_p^2 = \int_0^\infty \mathrm{Im}\,\varepsilon(\omega)\omega d\omega. \tag{5.3}$$

Calculation using (5.2) formula gives plasmon energy value of $\hbar\omega_p = 17.27\,\mathrm{eV}$ for the BiSeBr crystal and $\hbar\omega_p = 18.13\,\mathrm{eV}$ for the BiSBr crystal. Estimated plasmon energy using the sum rule gives very similar results. Plasmon energy calculations, according to (5.2) and (5.3) formulas, for BiSI, BiSeI, BiSCl, and for the others $A^{V}B^{VI}C^{VII}$ orthorhombic structure crystals gives the energy value approximately 1.5 eV lower than plasmon energy value found graphically.

5.3 Birefringence in the area of the ferroelectric phase transition

The refractive indices n_a, n_b and n_c were estimated along ***x***, ***y*** and ***z*** directions, respectively. The difference between two refractive indices at the same photon is about 0.5 in photon energy range from 2 to 6 eV. This difference between two refractive indices at the same photon energy vanishes in photon energy ranges from 0 to 2 eV and from 7 to 20 eV. All refractive indices spectra in the energy range from 0 to 14 eV have two large maxima. First refractive indices' maximum is in photon energy range from 0 to 5.8 eV and the second one is from 5.8 to 14 eV. In the range of first maximum (0 – 3 eV), the anisotropy of refractive indices n_a, n_b and n_c is very large, but in the energy range 3 7.5 eV, the anisotropy between n_b and n_c relation lowers. In the photon energy range from 12 to 20 eV, anisotropy of refractive indices vanishes because $n_a = n_b = n_c$.

The birefringence was calculated for SbSI crystal at fixed photon energies $E \approx 0$ eV and $E = 1.078$ eV ($\lambda = 1.15$ μm) in the 100 – 350 K temperature range (Fig. 16). The indices are approaching to linear above $T_c = 295$ K in paraelectric phase. The temperature where the indices depart from the linear behavior is denoted as phase transition temperature. In ferroelectric state, indices depend on spontaneous polarization P_s and have negative temperature dependence.

The linear refractive index increment $\Delta n_c = n_f - n_p$ is the increment of refractive indices induced at the transition. The Δn_c has been obtained by subtracting from the

linear temperature behavior of the n_p in the paraelectric phase andextrapolated to the ferroelectric phase (dashed lines in Fig. 16). The increments in Fig. 16 at the photon energy E = 1.078 eV and temperature T = 100 K have the values: $\Delta n_{c,\mathrm{S}} = 0.17$ along ***z***-axis direction and $\Delta n_{b,\mathrm{S}} = 0.12$ along ***y***-axis direction.

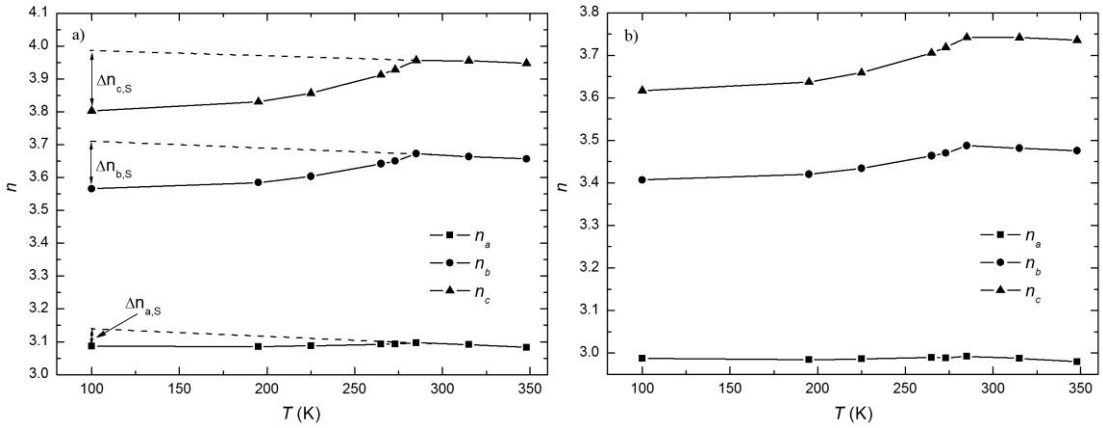

Fig. 16. Temperature dependence of the refractive indices n_a, n_b and n_c: a) when E = 1.078 eV and b) when $E \approx 0$ eV. The background lines are shown as dashed lines.

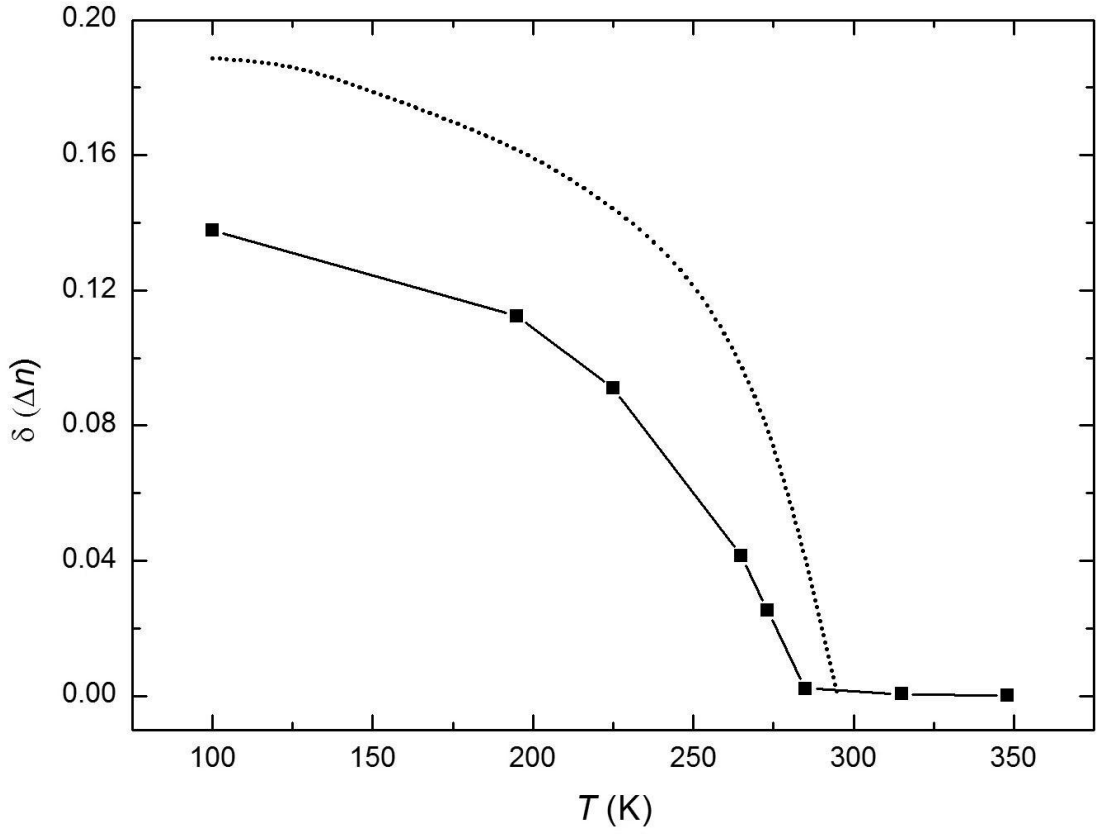

Fig. 17. Calculated linear birefringence increment $\delta(\Delta n)$ (solid line with square symbols) and experimental curve $\delta(\Delta n)_{\mathrm{exp}}$ (dots) [51] versus temperature. The laser energy is 1.078 eV.

For theoretical – experimental data comparison the theoretical linear birefringence increment $\delta(\Delta n = n_c - n_a)$ in ferroelectric phase has been obtained. In Figure 17, theoretical $\delta(\Delta n)$ and experimental $\delta(\Delta n)_{exp}$ comparison results are shown. Experimental curve $\delta(\Delta n)_{exp}$ is measured by high-frequency polarization modulation method described in Ref. [52]. Theoretical and experimental results are similar, the curves have the same tendency.

6 LATTICE DYNAMICS OF BiSI, SbSI AND SbSBr CRYSTALS

6.1 Investigation of phonon density of states

Dynamical properties of BiSI, SbSI and SbSBr crystals were obtained from a direct method [34, 53-56]. In this method, phonon frequencies were calculated from Hellmann-Feynman forces generated by nonequivalent atomic displacement in supercell. Each atom was displaced from its equilibrium position by 0.03 Å in Cartesian direction. Both positive and negative displacements were applied to minimize the systematic errors. The induced forces acting on all atoms within the supercell were used to construct the force constant matrix of the system. The phonon frequencies and the corresponding eigenvectors were obtained by diagonalizing the dynamical matrix. Thermal expansion is indirectly taken into account through calculation for various lattice volumes.

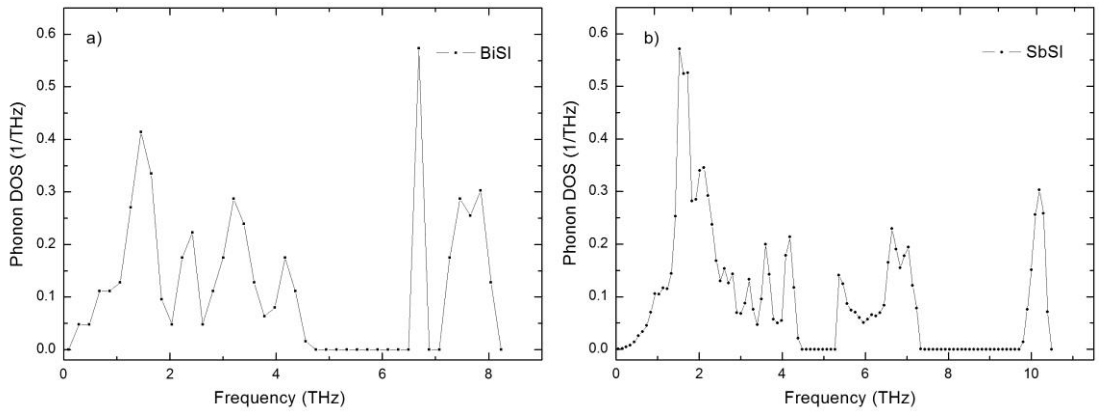

Fig. 18. The total phonon DOS in paraelectric phase: a) for BiSI crystal, b) for SbSI crystal.

The calculated total phonon DOS in paraelectric phase for BiSI and SbSI crystals are shown in Fig. 18. The dimensions of supercells were 1×1×1 for both crystals. For SbSI calculation the atomic coordinates and lattice parameters at 465 K temperature

were used [45, 46]. The total and partial phonon DOS in paraelectric phase at T = 30 K and ferroelectric phase at T = 11 K for SbSBr crystal were also calculated (the figures are given in the dissertation) [S10]. In all cases the amplitude of total phonon DOS does not exceed 0.65 T^{-1}. The results of partial phonon DOS for Sb, S and Br atoms in paraelectric and ferroelectric phases indicates that S atom has higher frequencies than Sb and Br atoms. The origin of the total phonon DOS peaks created by partial phonon DOS of SbSBr atoms in both phases are presented in Table 1.

Table 1. Origin of total phonon DOS peaks created by partial phonon DOS of SbSBr atoms in paraelectric phase at T = 30 K and ferroelectric phase at T = 11 K.

Range (in THz) of total phonon DOS peaks	The phonon DOS peaks created by partial phonon DOS of atoms	Axis direction
0 – 3	Sb, Br	***a(x), b(y), c(z)***
3.5 – 5	Sb, Br	***b(y)***
6 – 7.5	S	***c(z)***
7.5 – 8.5	S (90%), Sb (10%)	***b(y)***
10 – 10.5	S (90%), Sb (10%)	***a(x)***

6.2 Investigation of vibrational dispersion

Vibrational dispersion curves were calculated through the main points of the first Brillouin zone (Fig. 11), like in the electronic band structure studies. The highest accuracy of the calculation is obtained at the center of the Brillouin zone. If the calculations are inaccurate dispersion curves have imaginary parts (ie, a negative rate), usually it appears at Γ point or near it. Imaginary parts may appear due to two reasons: 1) the performed calculations are inaccurate or 2) studied compound is unstable. Instability creates a soft mode and therefore compounds undergo structural phase transitions [53-55]. Such instabilities can also be designed for high pressure [56]. However, although the compound has a phase transition it will not necessarily be obtained by imaginary parts. The phonon calculations evaluate only electron-phonon interaction, but do not take phonon-phonon interaction into account. For the crystal which has a phase transition the imaginary frequencies will be obtained if the phase transition is induced by the electron-phonon interaction.

The calculations for $A^{V}B^{VI}C^{VII}$ type orthorhombic structure crystals showed that dispersion curves obtained with 1×1×1 supercell are inaccurate. Figure 19 shows the BiSI crystal's dispersion curves calculated with 1×1×1 supercell. The imaginary parts arise at the Γ point of the Brillouin zone. However, there is evidence, that Bi atoms are too large and the anharmonicity is too small to induce a ferroelectric phase transition as in SbSI crystal [57]. Thus, these instabilities are due to inaccuracies of the calculation. Therefore, more precise calculations with increased supercell are needed.

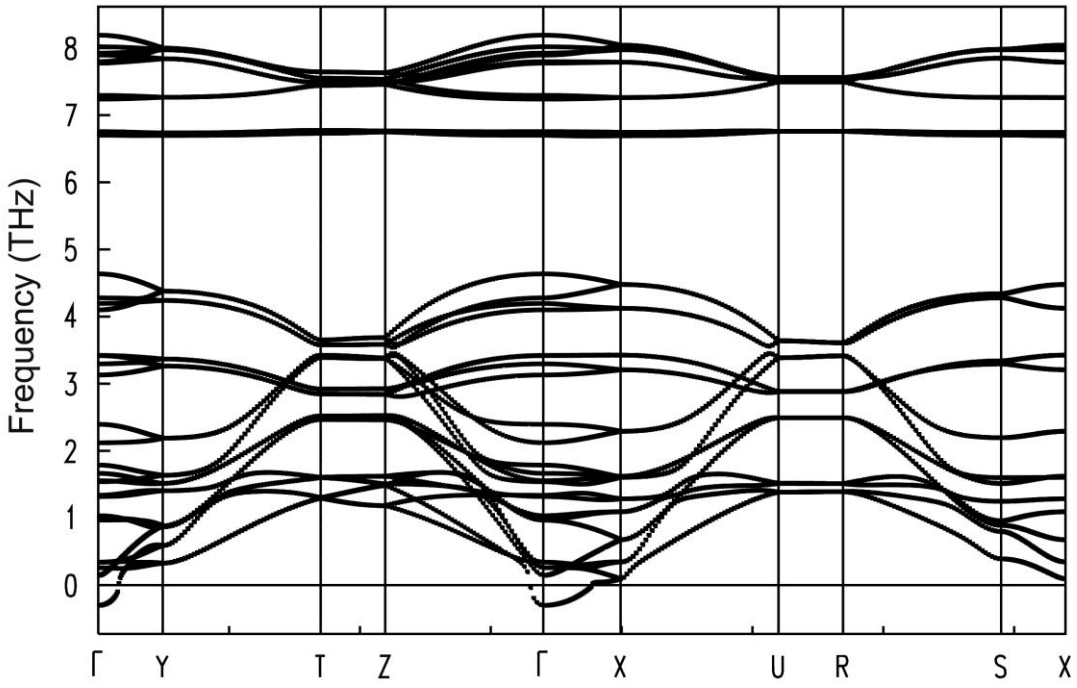

Fig. 19. The dispersion curves of the BiSI crystal in paraelectric phase.

Calculating the dispersion curves of the SbSBr crystal in paraelectric and ferroelectric phases with 1 × 1 × 1 supercell gives s small inaccuracies at the Γ point. The observed 36 modes, which some of them overlap on top of each other. The negative frequency is not high, it means the chosen supercell is too small. Therefore, we carried out more calculations by increasing the supercell. Figs. 20 and 21 show that increasing the supercell improves the result and negative frequency vanishes almost completely. Increasing in ***z***-axis direction does not give good results, providing even more imaginary

parts (Fig. 21a). However, the calculations with 2 × 2 × 1 supercell give the results with completely removed imaginary parts (Fig. 21b).

As is known, the SbSbr crystal has the ferroelectric phase transition (T_c = 22.8 K) and it is intermediate between order-disorder and displacement type (for the most part displacement type [58]). Electron-phonon interaction and Jahn-Teller effects contribute to this transition, but phonon-phonon interaction fulfils a fateful [58, 59]. Therefore, SbSBr dispersion curves do not yield negative phonon frequencies.

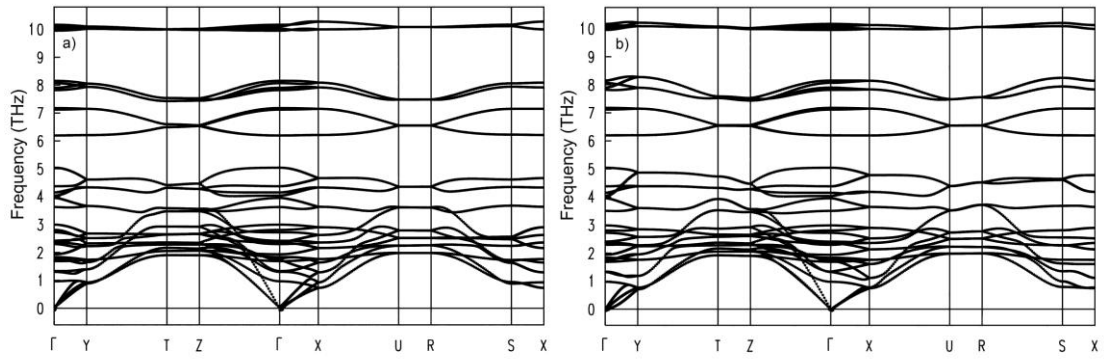

Fig. 20. The dispersion curves of the SbSBr crystal in paraelectric phase (30 K): a) supercell 2×1×1 and b) supercell 1×2×1.

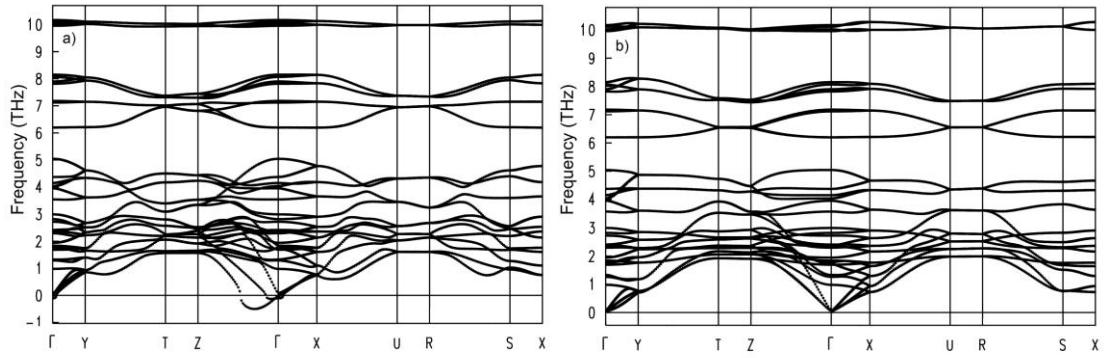

Fig. 21. The dispersion curves of the SbSBr crystal in paraelectric phase (30 K): a) supercell 1×1×2 and b) supercell 2×2×1.

7 THE VIBRATIONAL THERMODYNAMIC FUNCTIONS OF SbSI AND SbSBr CRYSTALS IN PARAELECTRIC AND FERROELECTRIC PHASES

7.1 Phonon free energy and mean-squared displacement of atoms in harmonic and quasiharmonic approximations

The free energy of the lattice vibration of the unit cell $F_{vib}(V,T)$ is calculated from the total phonon DOS using the formula [34]:

$$F_{vib}(V,T) = rk_BT\int_0^\infty g(\omega)\ln\left[2\sinh\left(\frac{\hbar\omega}{2k_BT}\right)\right]d\omega, \tag{7.1}$$

where *r* is the number of degree of freedom in the primitive unit cell, T – temperature, V – volume of the unit cell, $\omega = \omega(V)$ denotes the volume dependent phonon frequencies and $g(\omega)$ is the total phonon DOS, $\hbar$ is the Plank constant, and k_B is the Bolzmann constant.

Equation (7.1) contains some effect of anharmonicity since the phonon frequencies have to be derived each time at the current volume *V* of unit cell. A combination from any atom μ and degree of freedom *i* to the free energy of the unit cell is given by $F_{i,\mu}$.

$$F_{i,\mu} = rk_BT\int_0^\infty g_{i,\mu}(\omega)\ln\left[2\sinh\left(\frac{\hbar\omega}{2k_BT}\right)\right]d\omega \text{ and } F_{vib} = \sum F_{i,\mu}, \tag{7.2}$$

where $g_{i,\mu}$ is the partial phonon DOS which describes the contribution to the total DOS of the selected atom vibrating along selected Cartesian coordinate.

The knowledge of the lattice dynamics, the total $g(\omega)$ and partial $g_{i,\mu}(\omega)$ phonon DOS permits to calculate in quasiharmonic approximation the free energy of SbSI or SbSBr unit cell and contribution $F_{i,\mu}$ from Sb, S and Br atoms to the free energy along selected axis direction in paraelectric and ferroelectric phases.

The free energy of the unit cell F_{vib} and contribution from Sb, S and Br atoms to the free energy $F_{i,\mu}$ in ***z***-axis direction for a number of temperatures in harmonic and quasiharmonic approximations are plotted in Fig. 22.

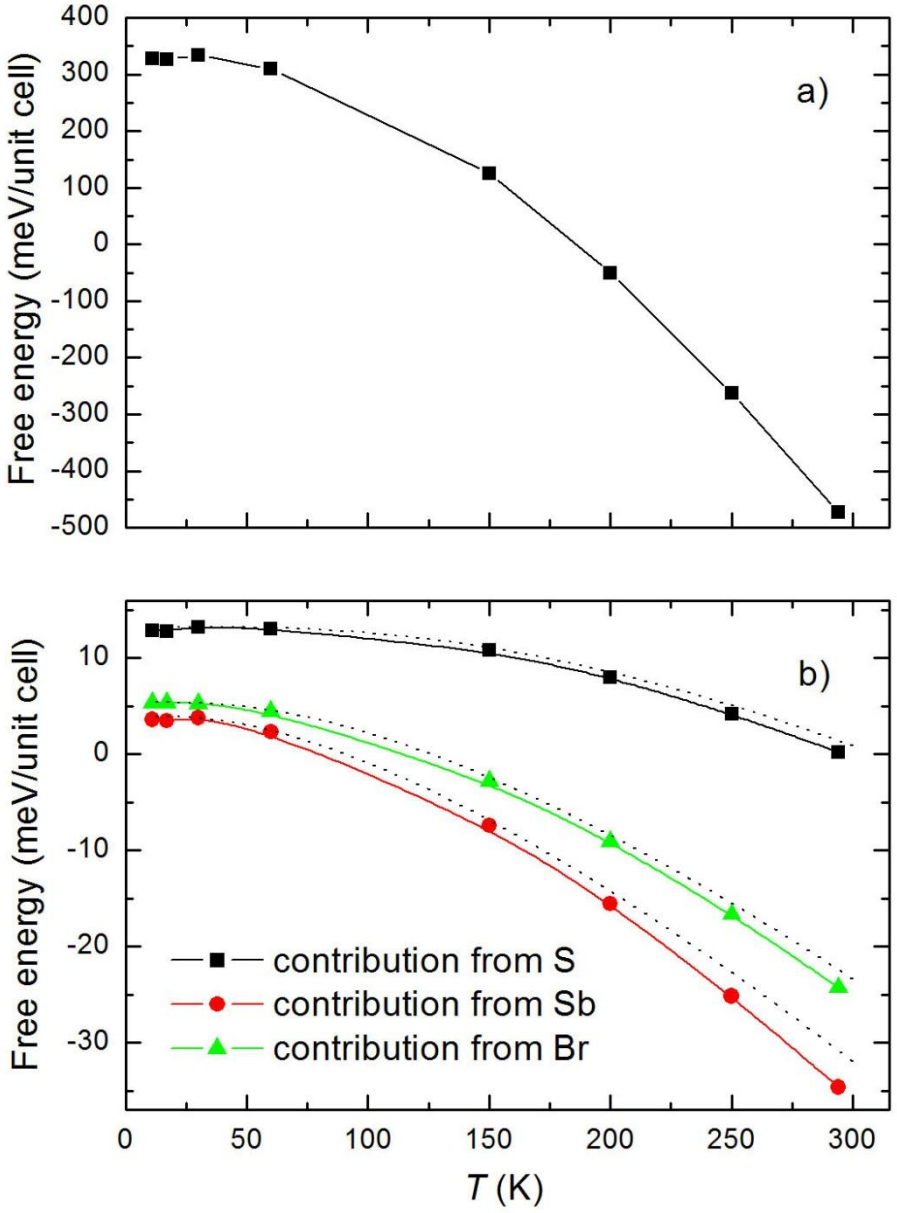

Fig. 22. a) Temperature dependence of the vibrational free energy of the unit cell of SbSBr crystal, b) Temperature dependence of contribution from Sb, S and Br atoms to the free energy along ***z***-axis direction. Dashed lines denote contribution in harmonic approximation.

As seen from Fig. 22 the temperature dependences of F_{vib} and of $F_{i,\mu}$ changes the slope with respect to the slope at T = 60 K. One of the possible reasons of the changes of the slope is the changes of total and partial DOS when temperature changes from 60 K to

11 K. The total and partial DOS have strong dependence on temperature because unit cell volume changes in paraelectric phase and Sb and S atoms shifts in ferroelectric phase.

The calculations reveal that deviations between the free energies of unit cell F_{vib} and contribution from atoms $F_{i,\mu}$ in quariharmonic approximation and free energies' in harmonic approximation with $g(\omega)$ and $g_{i,\mu}(\omega)$ at T = 60 K depend on temperature. The deviations changes from 5% to 15% increasing the temperature from 60 K to 294 K. The possible reason of these deviations is the changes of $g(\omega)$ and $g_{i,\mu}(\omega)$ when the temperature changes from 60 K to 294 K.

For investigation of anharmonisity along ***x***, ***y***, ***z***-axis directions in SbSBr crystal it is useful to calculate the mean-squared displacements of Sb, S and Br atoms.

A Debye-Waller factor in this case is defined as $\exp[-W\mu(\vec{k})]$, where $W\mu(\vec{k}) = 1/2[2\pi\vec{k} \cdot B(\mu) \cdot (2\pi\vec{k})]$, $B(\mu)$ is a second-rank symmetric tensor and represents the mean-squared displacement of atom μ. It is expressed by the diagonal and off diagonal partial phonon DOS of states $g_{iL,\mu}(\omega)$ taking the form [34]:

$$B_{iL,\mu}(\mu) = \frac{\hbar r}{2M\mu}\int_0^\infty g_{iL,\mu}(\omega)\cdot\omega^{-1}\coth\left(\frac{\hbar\omega}{2k_BT}\right)d\omega, \tag{7.3}$$

where M_μ is the mass of the atom μ and r is the number of degree of freedom in the primitive unit cell.

The temperature changes of the partial mean-square amplitudes $B_{i,\mu}$ of Br, S and Sb atoms in ***x***, ***y***, ***z***-axis directions are shown in Fig. 23. In the work of [60 (Fig. 6)] isotropic mean-square amplitude B of Sb, S and Br atoms in harmonic approximation is proportional to the absolute temperature in range from 100 K to 294 K. Supposing that the mean-square amplitudes $B_{i,\mu}$ of Sb, S and Br atoms in harmonic approximation are proportional to the absolute temperature in range from 100 K to 294 K, we have drawn tentatively the straight line passing through the origin and the value at 100 K.

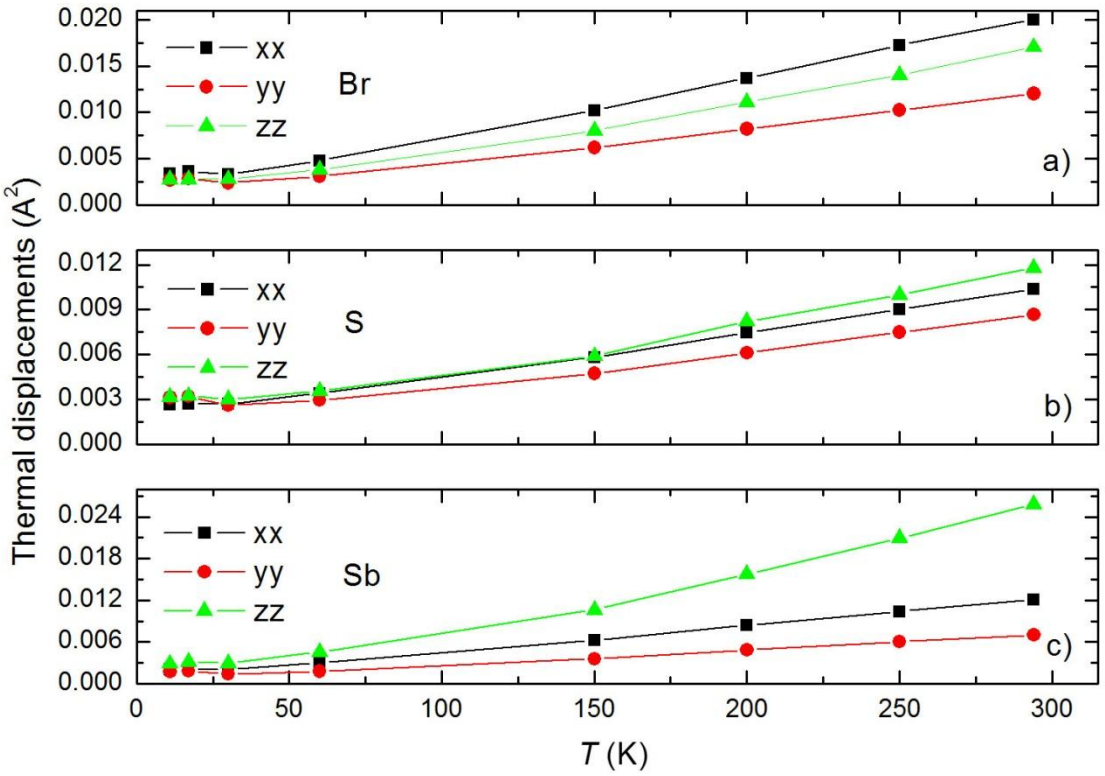

Fig. 23. Temperature dependence of the mean-square displacements $B_{i,\mu}$ along ***x***, ***y*** and ***z***-axis directions: a) for bromine, b) for sulphur and c) for antimony atoms.

For the Sb and S atoms, it is seen that values on the higher temperature side are located nearly on the straight line for ***x*** and ***y*** direction, except a large deviation in ***z*** direction. This fact indicates that the Sb atom vibrates harmonically in ***x*** and ***y*** directions over the temperature range 100 – 294 K. On the other hand the values B_z (Sb), B_z (S) in the temperature range 100 – 294K are all above the straight line. The slopes of temperature dependence of the mean-square displacements for B_z (Br), B_z (S) and B_z (Sb) in the region of ferroelectric phase from 22.8 K to 11 K are different from the slopes in the region of paraelectric phase from T_c = 22.8 K to 60 K. One of the possible reasons of difference of slopes of all $B_{z,\mu}$ near the transition temperature and strong changes of slope of B_z (Sb) and B_z (S) in the temperature range 100 – 294 K is the appearance of the intrinsic anharmonisity of potential energy of Sb and S atoms along ***z***-axis [59].

This consideration suggests that the observed deviation from the straight line is due to the softening effect of some phonon modes polarized along the ***z***-axis. Fig. 23c indicates that soft modes polarized along the ***z***-axis are observed over a wide temperature range and particularly observed near the transition point. The results, shown in Fig. 23, reveal that modes polarized along ***x*** and ***y*** directions indicate no softening behavior in temperature range from 100 K to 294 K. The possible reason for the softening effect of phonon along ***z***-axis is the change of $g_{i,\mu}(\omega)$ created by temperature dependence of the unit cell constant c in paraelectric phase. Further, by the shift of Sb and S atoms along ***z***-axis in ferroelectric phase.

7.2 Helmholtz free energy, internal energy and entropy in the range of ferroelectric phase transition

The vibrational contribution of free energy equals: $F_{vib}(V,T) = U(V,T) - TS(V,T)$, where $U(V,T)$ describes the internal energy of the lattice including zero-point vibrations, while the last term is for the entropic contribution. The internal energy $U(V,T)$ and entropy $S(V,T)$ of the unit cell equals [34, 53]:

$$U(V,T) = \frac{1}{2} r \int_0^\infty g(\omega)(\hbar\omega) \coth\left(\frac{\hbar\omega}{2k_B T}\right) d\omega, \tag{7.4}$$

$$S(V,T) = r k_B \int_0^\infty g(\omega) \left\{ \left(\frac{\hbar\omega}{2k_B T}\right) \left[\coth\left(\frac{\hbar\omega}{2k_B T}\right) - 1 \right] - \ln\left[1 - \exp\left(-\frac{\hbar\omega}{k_B T} \right) \right] \right\} d\omega. \tag{7.5}$$

The Helmholtz free energy *F*, of the crystal is a sum of a ground state energy *E* and the free energy of the lattice vibration F_{vib}: $F = E + F_{vib}$. The difference of the free energy of the lattice vibration ΔF_{vib} is calculated as follows: $\Delta F_{vib} = \Delta U - T\Delta S$ or $\Delta E + \Delta F_{vib} = (\Delta E + \Delta U) - T\Delta S$, or $\Delta F = (\Delta E + \Delta U) - T\Delta S$ [53].

Comparing the temperature-dependent free energies of the f (ferroelectric) and p (paraelectric) phases, it is possible to obtain the phase transition temperature. Further two total energy (ground state energy) calculations as functions of the unit cell volume *V* at both phases are necessary to perform. The total energy as a function of the volume *V*

may be calculated using WIEN2k [29]. The difference between the corresponding total energy minima at 11 K (ferroelectric phase) and 294 K (paraelectric phase) gives the ground state energy $\Delta E_{f-p} = 2\,\text{meV}$ per unit cell. The differences of the Helmholtz free energy (ΔF_{f-p}), internal energy ($\Delta E_{f-p} + \Delta U_{f-p}$), and entropy term ($T\Delta S_{f-p}$) between f and p phases on temperature are shown in Fig. 24.

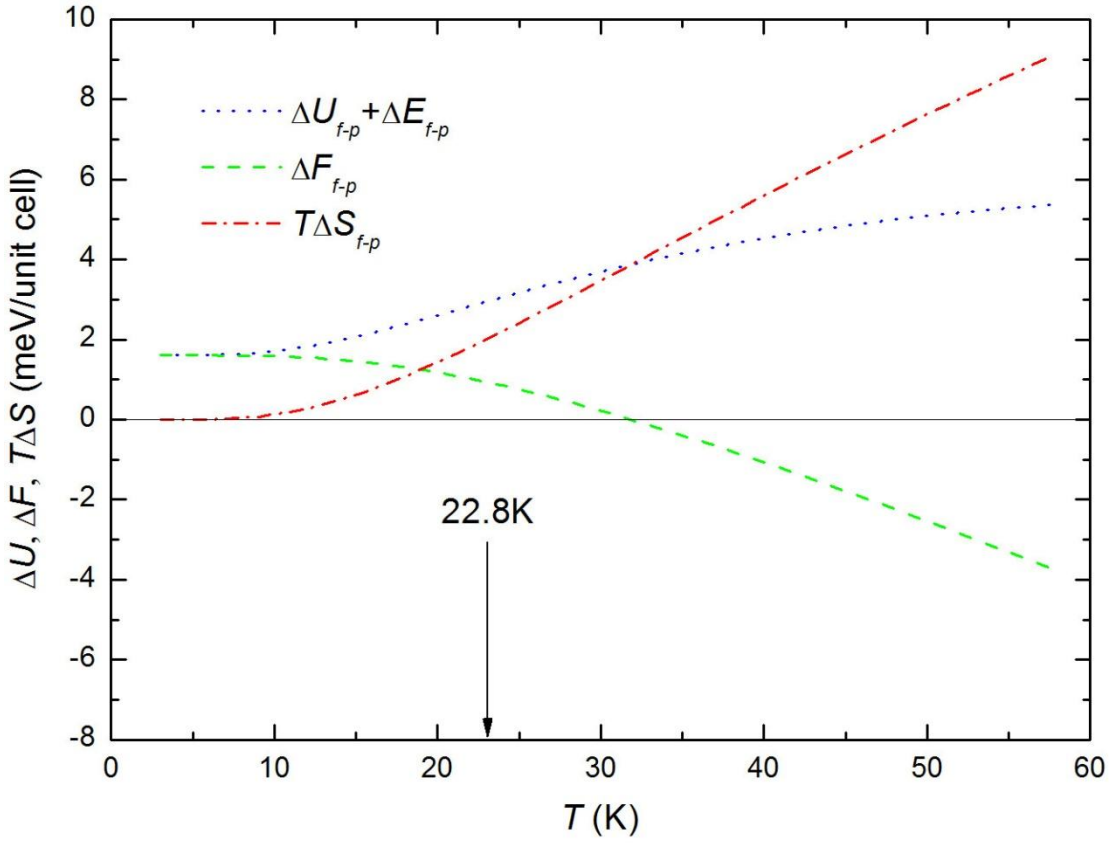

Fig. 24. Difference of the Helmholtz free energy, internal energy, and entropy term between f and p phases on temperature.

The values for the paraelectric phases are used as a reference line. From Figure 24, it follows that the paraelectric phase is more stable than ferroelectric phase since the Helmholtz free energy in the paraelectric phase is lower. The entropy favors the SbSBr structure, whereas the internal energy has only little impact on phase stability of the phase, driving the SbSBr to be more stable above 30 K. The obtained transition temperature is close with measured value of T_c = 22.8 K. It is possible to get exact value with lower ground state energy $\Delta E_{f-p} = 1\,\text{meV}$ per unit cell. The reason why there is no

perfect congruence is the fact that the crystal dynamic is characterized by a collection of noninteracting harmonic oscillators (7.1) – (7.5).

7.3 Influence of the anharmonicity for the SbSI and SbSBr thermodynamic functions

SbSI and SbSBr crystals in the paraelectric phase have the soft mode B_{1u} (A_1). Its frequency varies according to the formula $\omega_{TO}^2 = \omega_s^2 = A(T - T_c)^{\gamma'}$, where $\gamma' = 1$ is the mean field critical exponent. The soft mode B_{1u} gives the main contribution to the static dielectric permittivity $\varepsilon(0) = \Delta\varepsilon + \varepsilon_\infty$ near the T_c temperature [2]. This soft mode has two components: a soft mode in the microwave range [57] and the soft mode in the infrared (IR) spectrum range. Both components are due to atomic movement in the potential field V (***z***) and persist as long as there is an interaction between the chains. If the interaction between the chains disappears, no presents of the soft mode component in the microwave range can be detected [61]. In our case the soft mode is maintained and it can be described by an anharmonic oscillator vibrating in a double-well potential energy expressed [58, 59] as follows:

$$V = bz^2 + cz^4, \tag{7.6}$$

where, *z*'s are displacements of atoms from their equilibrium positions in B_{1u} symmetry normal mode and *b* and *c* the parameters of soft mode (*b* < 0, *c* > 0). The factor $\Delta V = b^2/4c$ characterizes a barrier between two maxima of a double-well potential energy. The term cz^4 depends on the interaction between the anharmonic oscillator of B_{1u} symmetry with other oscillators of the same symmetry. Because the phase transition in SbSBr crystal exhibits an intermediate behavior between displacive and order – disorder nature, the phase transition temperature may be found by means of the equation $k_B T_c^{anh} \approx \Delta V_c$. In the literature [58, 59] it is found that T_c^{anh} approximately equals to the experimental value T_c = 22.8 K. Therefore we assume, that noninteracting phonons drive the temperature of phase transition to $T_c^{anh} \approx 30\,\mathrm{K}$, but interacting anharmonic oscillators drive the phase transition temperature to the experimental value T_c = 22.8 K.

8 INVESTIGATIONS OF THE DIELECTRIC PROPERTIES

SbSI and SbSeI crystals were grown by the common Bridgman–Stockbarger technique. Further, they were cut into tablets 4 mm thick perpendicular to the longitudinal axis by a diamond disk and then polished. The capacitance was measured in the midst of the conductive temples at frequency of 1 kHz. Such a frequency is set because of an increase in capacitance values at lower frequencies [62]. Measurement details are given in the dissertation.

In the International System of Units, variation of the capacitance C leads to the dielectric permittivity changes and it is based on the equation:

$$C = \frac{\varepsilon \cdot \varepsilon_0 S}{d}, \tag{8.1}$$

where S is the contact area, d is the distance between the contacts, $\varepsilon_0 = 8{,}85 \cdot 10^{-12}$ F/m.

Results obtained for SbSI crystals are presented in Fig. 25. As discussed in [31, 32, 63] from X-ray studies above the high temperature phase transition that exists at 410 K. Only then does the SbSI crystal become centrosymmetric. Certainly SbSI has three phases: ferroelectric (T < 298 K), antiferroelectric (298 K < T < 410 K) and paraelectric (T > 410 K). As established in Ref. [62], BiSeI exhibits an increase of the dielectric permittivity and AC conductivity giving a peak at the temperature of 410 K. Our capacitance (dielectric permittivity) measurements for SbSeI crystals also confirm the existence of a peak near the considerable temperature. For SbSeI and SbSI crystals the position of this peak depends on heating and cooling rate. Following an increase in capacitance (dielectric permittivity) propose a new antiferroelectric phase transition as in SbSI crystals. Therefore, we come to the conclusion that BiSeI, SbSeI and SbSI are in antiferroelectric phase when T < 410 K and in paraelectric phase when T > 410 K. All these crystals have antiferroelectric phase transition near the 410 K temperature. Under this transition the antiferroelectric phase changes to the paraelectric phase.

Ferroelectricity and phase transitions in SbSI are closely related to its equilibrium positions of the atoms in the elementary unit cell, lattice parameters and phonon interaction which depends on temperature. This interaction changes the form of the soft

mode potential energy and thus changes the soft mode behavior, temperature of ferroelectric phase transition and its order [63]. In the antiferroelectric phase, equilibrium positions of the atoms in the elementary unit cell and lattice parameters of the soft mode differs from the equilibrium positions of the atoms in the elementary unit cell and lattice parameters of the soft mode in the ferroelectric phase. Ferroelectric phase transition in the SbSI is related to B_{1u} soft mode at Brillouin zone point k = 0, when the antiferroelectric phase transition near the 410 K temperature is related to the B_{1u} soft mode at Brillouin zone point $k = \pi/c$. Because the electronic potential energy of soft mode in the antiferroelectric phase is double-well form, the mode is very low frequency. Therefore, the authors of work [63] did not observe any change of permittivity at frequency of 30 GHz.

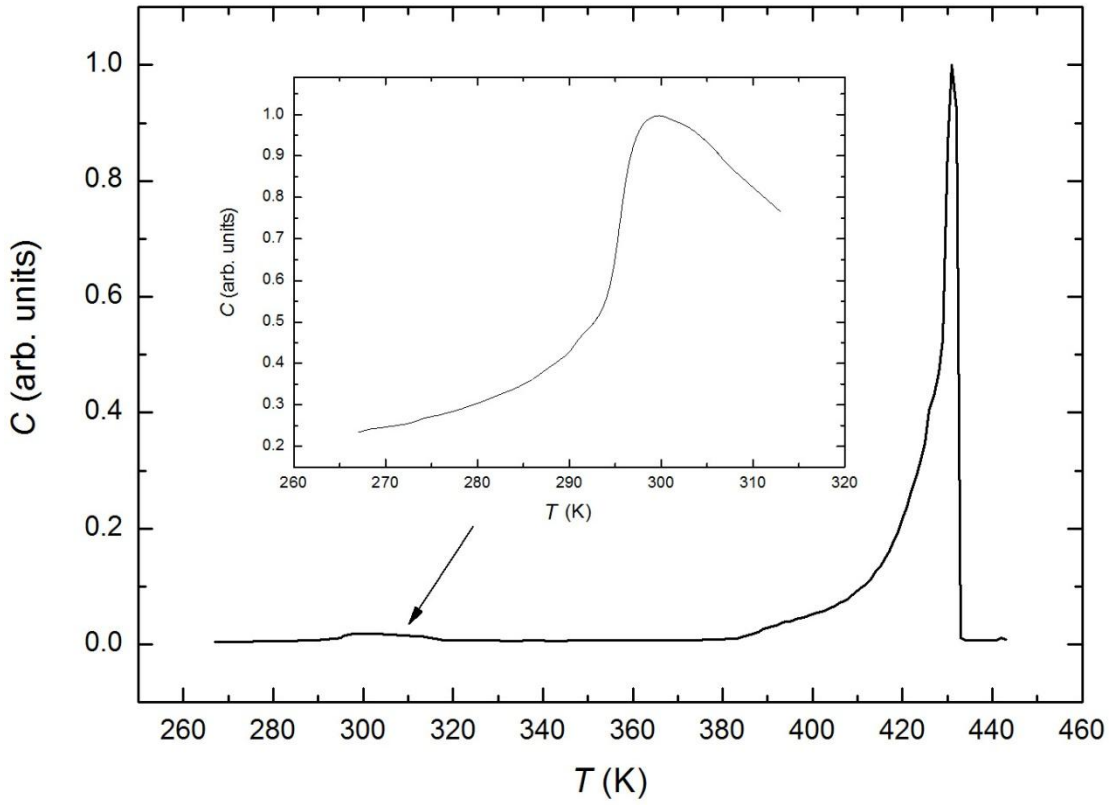

Fig. 25. Variation of capacitance with temperature for SbSI crystals at frequency – 1 kHz when a sample is heated. The inset shows ferroelectric phase transition peak. $S = 1$ cm^2, $d = 4$ mm.

GENERAL CONCLUSIONS

1. The calculated electron charge density distribution confirms that the orthorhombic structure $A^{V}B^{VI}C^{VII}$ crystals' atoms have covalent type chemical bonds with a greater or lesser ionicity factor.
2. $A^{V}B^{VI}C^{VII}$ type semiconductor crystals have three or four valence bands mainly composed of A^{V} atom's s/p, B^{VI} atom's s/p and C^{VII} atom's s/p hybridized orbital. The lowest conduction band is mainly composed of A^{V} atom's p orbital. $A^{V}B^{VI}C^{VII}$ type crystals are characterized by the non-linear band gap with an indirect transition from Z – Γ to Γ point. Direct transition take place from Γ to Γ. Theoretical calculations of the electronic structure of the DFT approach in most cases is quite close to the experimental values and confirm the results of the other authors.
3. Theoretically, with the DFT method, calculated dielectric functions ε_{re} and ε_{im} are sufficiently in a good agreement with the experimental data, which were obtained using an optical spectrum ellipsometer from 1.5 to 5 eV. Experimental results are also well described by the pseudo-dielectric function with three or four Lorentz-type oscillators. Optical $n(E)$, $k(E)$, $L(E)$, $K(E)$ and $R(E)$ spectra show two intense, large maxima, which are composed of smaller peaks. These maxima caused by the optical transitions that take place from the p and s orbital in the valence band to the conduction band. Plasmon energy calculations showed that the orthorhombic structure $A^{V}B^{VI}C^{VII}$ crystals' plasmon energy value from 16 to 20 eV. Theoretical SbSI crystal's refractive indices and birefringence study showed that the refractive indices increments $\Delta n_{c,S}$, $\Delta n_{b,S}$ and the birefringence increment $\delta(\Delta n)$ in the ferroelectric phase depends on the spontaneous polarization P_s. Theoretical $\delta(\Delta n)$ and experimental $\delta(\Delta n)_{exp}$ birefringence results are similar.
4. The total phonon density of states for BiSI, SbSI and SbSBr crystals are distributed in the frequency range from 0 to 10.5 THz. The spectrum of partial phonon DOS of Sb and Br atoms mainly distributes below 5 THz and has six

large peaks. The spectrum of the partial phonon DOS of S atoms mainly exits higher than 6 THz and also has six large peaks. The vibrational dispersion study confirms that the electron-phonon interaction has a little impact on the SbSBr ferroelectric phase transition.

5. In the SbSBr ferroelectric phase $T < T_c$ = 22.8 K the temperature dependence of F_{vib} and $F_{i,\mu}$ changes the slope with respect to the slope at 60 K in paraelectric phase. The difference of slopes in ferroelectric phase ($T < T_c$ = 22.8 K) and paraelectric phase from T_c to 60 K is created by strong temperature dependence of the unit cell volume in paraelectric phase and shift of Sb and S atoms along ***z***-axis in ferroelectric phase. Investigation of mean-squared displacements of Sb, S and Br atoms in ***x***, ***y*** and ***z*** direction in quasiharmonic approximation in paraelectric and ferroelectric phases indicates that Sb and S atoms vibrates harmonically in ***x*** and ***y*** direction over the temperature range 100 – 294 K. But Sb and S atoms vibrates anharmonicaly in ***z***-axis direction over the temperature 100 – 294 K and in transition range from 11 to 60 K. The possible reason for the softening effect of phonons along ***z***-axis is the change of total phonon DOS and partial phonon DOS created by strong temperature dependence of the lattice constant c in paraelectric phase and shift of Sb and S atoms along ***z***-axis in ferroelectric phase. It is shown that entropy favors the SbSBr structure, where the internal energy has little impact on phase stability. It is established that the paraelectric phase is more stable than ferroelectric phase since the Helmholtz free energy in the paraelectric phase is lower. The obtained ferroelectric phase transition temperature is in reasonable agreement with the experimental value.
6. BiSeI, SbSI and SbSeI crystals in the temperature dependent dielectric spectra have a sharp peak at the temperature $T \sim 410$ K. Temperature dependence of permittivity (electrical capacitance) depends on the temperature dependence of frequency of soft mode in double-well potential energy $V(\boldsymbol{z})$ in the antiferroelectric phase. But in paraelectric phase, the temperature dependence of permittivity exhibits a strong drop according to the changes of soft mode double-

well potential energy to a single-well potential energy. These changes are affected by equilibrium atomic positions of the elementary unit cell, lattice parameters and the phonon interaction changes. SbSI crystal has three phases: ferroelectric (T < 298 K), antiferroelectric (298 K < T < 410 K) and paraelectric (T > 410 K). BiSeI and SbSeI crystals have two phases: antiferroelectric (T < 410 K) and paraelectric (T > 410 K).

REFERENCES

1. E. I. Gerzanich and V. M. Fridkin, *AVBVICVII type Ferroelectrics* (Nauka, Moskva, 1982).
2. J. Grigas, *Microwave Dielectric Spectroscopy of Ferroelectrics and Realated Materials* (Gordonand Breach Publisher, OPA Amsterdam, 1996).
3. E. Fatuzzo, G. Harbeke, W. J. Merz, R. Nitsche, H. Roetschi and W. Ruppel, *Ferroelectricity in SbSI*, Phys. Rev. **127** (6), 2036-2037 (1962).
4. V. Fridkin, *The First Observation of the Tricritical Point in Ferroelectrics*, Ferroelectrics **354** (1), 259-264 (2007).
5. J. F. Li, D. Viehland, A. S. Bhalla and L. E Cross, *Pyro-optic studies for infrared imaging*, J. Appl. Phys. **71** (5), 2106-2113 (1992).
6. S. Kotru, W. Liu, R. K. Pandey, *PLD growth of high vapor pressure antimony sulpho-iodide ferroelectric films for IR applications*, Proceedings of the 12th IEEE International symposium on Applications of Ferroelectrics, 231 (2001).
7. S. Surthi, S. Kotru, R. K. Pandey, *SbSI films for ferroelectric memory applications*, Integr. Ferroelectrics **48** (1), 263-269 (2002).
8. Y. Xu, F. Del Monte, J. D. Mackenzie, K. Namjoshi, P. Muggli, C. Joshi, *Nanocomposite of semiconducting ferroelectric antimony sulphoiodide dot-doped glasses*, Ferroelectrics **230** (1), 11-20 (1999).
9. Y. Xu, C. H Cheng, Y. Hui, J. D. Mackenzie, *Electro-optic effect in a nanocrystals doped glass*, Ferroelectrics **259** (1), 259-268 (2001).

10. Y. Hui, X. Yuhuan and J. D. Mackenzie, *Semiconducting ferroelectric SbSI quantum dots in organically modified TiO_2 matrix*, Proc. SPIE 3943 95-101 (2000).
11. C. Wang, K. Tang, Q. Yang, B. Hai, G. Shen, C. An, W. Yu, Y. Qian, *Synthesis of novel SbSI nanorods by hydrothermal method*, Inorg. Chemi. Commun. **4** (7), 339-341 (2001).
12. A. V. Gomonnai, Yu. M. Azhniuk, Yu. M. Vysochanskii, I. P. Prits, I. M. Voynarovych, M. M. Maior, V. V. Lopushansky, *Raman scattering in chalcogenide-based ferroelectrics: from bulk to nanoscale*, Phys. Stat. Sol. (c) **1** (11), 3166-3169 (2004).
13. M. Nowak, P. Szperlich, Ł. Bober, J. Szala, G. Moskal, D. Stróż, *Sonochemical preparation of SbSI gel*, Ultrason. Sonochem. **15** (5), 709-716 (2008).
14. M. Nowak, P. Szperlich, E. Talik, J. Szala, T. Rzychoń, D. Stróż, A. Nowrot, B. Solecka, *Sonochemical preparation of antimony subiodide*, Ultrason. Sonochem. **17** (1), 219-227 (2010).
15. L. Zhu, X. Zheng, X. Yin, X. Tian, *Growth of Compound Bi^{III}-VI^{A}-VII^{A} Crystals with Special Morphologies under Mild Conditions*, Inorg. Chem. **41** (17), 4560-4566 (2002).
16. Z. T. Deng, D. Chen, B. Peng and Q. F. Tang, *From Bulk Metal Bi to Two-Dimensional Well-Crystallized BiOX (X = Cl, Br) Micro- and Nanostructures: Synthesis and Characterization*, Cryst. Growth Des. 8 (8), 2995-3003 (2008)
17. F. Fang, C. Ling, W. Li-Ming, Syntheses, *Morphologies and Properties of BiOI Nanolamellas and BiSI Nanorods*, Chinese J. Struct. Chem. **28** (11), 1399-1406 (2009).
18. Z. Deng, F. Tang, A. J. Muscat, *Strong blue photoluminescence from single-crystalline bismuth oxychloride nanoplates*, Nanotechnology **19** (29), 295705 (2008).
19. J. Ma, X. Liu, J. Lian, X. Duan, W. Zheng, *Ionothermal Synthesis of BiOCl Nanostructures via a Long-Chain Ionic Liquid Precursor Route*, Cryst. Growth Des. **10** (6), 2522-2527 (2010).

20. K. L. Zhang, C. M. Liu, F. Q. Huang, C. Zheng, W. D. Wang, *Study of the electronic structure and photocatalytic activity of the BiOCl photocatalyst*, Appl. Catal. B **68** (3-4) 125-129 (2006).
21. C. Wang, C. Shao, Y. Liu, L. Zhang, *Photocatalytic properties BiOCl and Bi_2O_3 nanofibers prepared by electrospinning*, Scr. Mater. **59** (3), 332-335 (2008).
22. E. Dönges, *Über Thiohalogenide des dreiwertigen Antimons und Wismuts*, Z. Anorg. Allg. Chem. **263** (1-3), 112-132 (1950).
23. F. Skuban, S. R. Lukic, D. M. Petrovic, I. O Gúth, *Refractive-index dispersion of glassy semiconductors in the pseudo-binary As_2Se_3–SbSI system*, J. Non-Cryst. Solids **355** (1), 2059-2062 (2009).
24. V. M. Rubish, M. Yu. Rigan, S. M. Gasinets, O. V. Gorina, D. I. Kaynts, V. V. Tovt, *Obtaining and Crystallization Pecularities of Antimony Containing Chalcohalogenide Glasses*, Ferroelectrics **372** (1), 87-92 (2008).
25. Y. Porat and R. Y. Ting, *The piezoelectric and dielectric properties of $SbSI(Sb_2S_3)_x$ composites*, Ferroelectrics **87** (1), 155-165 (1988).
26. B. Garbarz-Glos, *Dielectric Properties of SbSI-Modifed in Phase Transition Region*, Ferroelectrics **292** (1), 137-143 (2003).
27. J. Grigas, A. Kajokas, A. Audzijonis, L. Žigas, *Peculiarities and properties of SbSI electroceramics*, J. Eur. Ceram. Soc. **21** (10), 1337-1340 (2001).
28. S. Cottenier, *Density Functional Theory and the family of (L)APW-methods: a step-by-step introduction* (Belgium: Insti-tuut voor Kern-en Stralingsfysica, K. U. Leuven, 2004).
29. P. Blaha, K. Schwarz, G. Madsen, D. Kvasnicka, J. Luitz, *WIEN2k. An Augmented Plane Wave Plus Local Orbitals Program for Calculating Crystal Properties* (Techn. Universitat Wien, Austria, 2001).
30. J. P. Perdew, K. Burke, M. Ernzerhof, *Generalized Gradient Approximation Made Simple*, Phys. Rev. Lett. **77** (18), 3865-3868 (1996).
31. R. M. A. Azzam and N. M. Bashara, *Ellipsometry and Polarized Light* (North-Holland, Amsterdam, 1977).
32. A. Galickas, *Regression analysis in experimental technique*, Lithuanian J. Phys. **39** (2), 149-153 (1999).
33. А. В. Ржанов, *Основы элипсометрии* (Наука, Новосибирск 1979).

34. K. Parlinski, *Software Phonon* (Institute of Nuclear Physics, Cracow, 2008).
35. C. Y. Fong, C. Perlov and F. Wooten, *Electronic properties of BiSeI and BiSeBr*, J. Phys. C: Solid State Phys. **15** (12), 2605-2612 (1982).
36. E. Furman, O. Brafman and J. Makovsky, *Approximation to long-wavelength lattice dynamics of SbSI-type crystals*, Phys. Rev. B **13** (4), 1703-1710 (1976).
37. K. Unger, H. Neumann, *The Antisymmetric Gap and the Total Width of the Valence Band of Binary Compound Crystals*, Phys. Stat. Sol. (b) **64** (1), 117-122 (1974).
38. L. Pauling, *The Nature of the Chemical Bond and the Structure of Molecules and Crystals* (Cornell University Press, New York, 1960).
39. W. Schröter, K. H. Lautenschläger, H. Bibrack, A. Schnabel. *Chemie*. (Veb Fachbuchverlag, Leipzig, 1986).
40. J. J. Yeh and I. Lindau, *Atomic subshell photoionization cross sections and asymmetry parameters: 1 ⩽ Z ⩽ 103*, At. Data Nucl. Data Tables **32** (1), 1-155 (1985).
41. J. Grigas, E. Talik and V. Lazauskas, *Splitting of the XPS in Ferroelectric SbSI Crystals*, Ferroelectrics **284** (1), 147-160 (2003).
42. J. Grigas, E. Talik, M. Adamiec, V.Lazauskas and V. Nelkinas. *XPS and electronic structure of quasi-one-dimensional BiSI crystals*. J. Electron. Spectrosc. Relat. Phenom. **153** (1-2), 22-29 (2006).
43. H. Akkus, A. M. Mamedov, *Ab-initio calculation of band structure and linear optical properties of SbSI in para- and ferroelectric phases*, Centr. Eur. J. Phys. **5** (1), 25-34 (2007).
44. H. Akkus, A. M. Mamedov, *Ab initio calculations of the electronic structure and linear optical properties, including self-energy effects, for paraelectric SbSI*, J. Phys.: Condens. Matter **19** (11), 116207-116217 (2007).
45. K. Łukaszewicz, A. Pietraszko, J. Stepien-Damm, A. Kajokas, *Crystal Structure and Phase Transitions of the Ferroelectric Antimony Sulfoiodide SbSI. Part I. Phase Diagram and Thermal Expansion of SbSI*, Polish J. Chem. **71** (9), 1345-1349 (1997).
46. K. Łukaszewicz, A. Pietraszko, J. Stepien-Damm, A. Kajokas, *Crystal Structure and Phase Transitions of the Ferroelectric Antimony Sulfoiodide SbSI. Part II.*

Crystal Structure of SbSI in Phases I, II and III, Polish J. Chem. **71** (9), 1852-1857 (1997).

47. S. A. Park, M. Y. Kim, J. Y. Lim, B. S. Park, J. D. Koh, W. T. Kim, *Optical Properties of Undoped and V-Doped VA−VIA−VIIA Single Crystals*, Phys. Stat. Sol. (b) **187** (1), 253-260 (1995).
48. K. Kreher, *Ferroelectric Semiconductors,* Wiss. Z. Karl-Marx – Univ. Leipzig, Math-Naturwiss **20**, 287-301 (1971).
49. H. Akkus, *Density Functional Calculation of the Electronic Structures of Some $A^5B^6C^7$-Type Crystals*, Int. J. Mod. Phys. B **23** (1), 97-104 (2009).
50. H. R. Philipp, H. Ehrenreich, *Optical Properties of Semiconductors*, Phys. Rev. **129** (4), 1550-1560 (1963).
51. K. Žičkus, A. Audzijonis, J. V. Gurvič, A. Kindurys and J. Lipavičius, *Hydrostatic Pressure Effect on The Absorption Edge of HGS-2 Crystal*, Solid State Phys. **27**, 1261-1262 (1985).
52. D. J. Benard and W. C. Walker, *Modulated Polarization Measurement of Structural Phase Transitions in KMnF3*, Rev. Sci. Instrum. **47** (1), 122-127 (1976).
53. Z. Łodziana and K. Parlinski, *Dynamical stability of the α and θ phases of alumina*, Phys. Rev. B **67** (17), 174106-174113 (2003).
54. K. Parlinski and M. Parlinska-Wojtan *Lattice dynamics of NiTi austenite, martensite, and R phase*, Phys. Rev. B **66** (6), 064307-064315 (2002).
55. D. Góra and K. Parlinski, *Ab initio calculation of $Ni_{50-x}Fe_xTi_{50}$*, J. Phys. Chem. Solids **66** (10), 1748-1754 (2005).
56. J. Łażewski, P. T. Jochym, P. Piekarz and K. Parlinski, *Quasiharmonic approach to a second-order phase transition*, Phys. Rev. B **70** (10), 104109-104116 (2004).
57. S. Kvedaravičius, A. Audzijonis, N. Mykolaitienė and J. Grigas, *Soft mode and its electronic potential in SbSI-type mixed crystals*, Ferroelectrics **177** (1), 181-190 (1996).
58. A. Audzijonis, L. Žigas, J. Siroicas, J. Narušis, R. Žaltauskas, A. Pauliukas, A. Čerškus and R. Šadžius, *Investigation of the Soft Mode of $SbSBr_xI_{1-x}$ Crystals*, Ferroelectrics **300** (1), 15-31 (2004).

59. S. Kvedaravičius, A. Audzijonis, N. Mykolaitienė and A. Jancerevičius, *The electronic potential of the V-VI-VII compounds in the region of phase transition*, Phase Trans. **58** (4), 235-246 (1996).
60. T. Inushima, *X-ray study of crystal structure and diffuse scattering spectra of ferroelectric SbSBr having pseudo-Jahn–Teller phase transition*, J. Phys. Chem. Solids **60** (5), 587-598 (1999).
61. J. W. Flocken, R. A. Guenther, J. R. Hardy, L. L. Boyer, *A double well oscillator model for the ferroelectric phase transition in SbSI*, Ferroelectrics, **135** (1), 309-318 (1992).
62. R. Ganesha, D. Arivuoli, P. Ramasamy, *Growth of some group V-VI-VII compounds from the vapour*, J. Cryst. Growth **128** (1-4), 1081-1085 (1993).
63. A. Audzijonis, J. Grigas, A. Kajokas, S. Kvedaravičius and V. Paulikas, *Origin of ferroelectricity in SbSI*, Ferroelectrics **219** (1), 37-45 (1998).

APPROBATION OF THE RESULTS

The author has published 18 scientific publications, 13 of them are directly connected with the topic of the dissertation and are included in the database of the Institute of Scientific Information (ISI). The results were also presented in 13 International, National scientific conferences and seminars. 7 of them are directly connected with the topic of the dissertation.

Scientific publications of the author on the topic of the dissertation

Publications in the journals included in the database of the Institute of scientific Information (ISI).

S1. A. Audzijonis, A. Rėza, R. Žaltauskas, L. Žigas, R. Sereika, C. Paškevič, A. Pauliukas, *Spectroscopic ellipsometry studies of ferroelectric $SbSe_xS_{1-x}I$ crystals*, Ferroelectrics. ISSN 0015-0193. Vol. 366 (2008), p. 45-54.

S2. A. Audzijonis, R. Sereika, R. Žaltauskas, *Antiferroelectric phase transition in SbSI and SbSeI crystals*, Solid State Communications. ISSN 0038-1098. Vol. 147, no. 3/4 (2008), p. 88-89.

S3. A. Audzijonis, L. Žigas, R. Žaltauskas, R. Sereika, A. Pauliukas, *Origin of the optical anomalies near the ferroelectric phase transition in SbSI and SbSBr crystals*, Ferroelectric Letters. ISSN 0731-5171. Vol. 35 (2008), p. 51-61.

S4. A. Audzijonis, G. Gaigalas, L. Žigas, R. Sereika, R. Žaltauskas, D. Balnionis, A. Rėza, *Electronic structure and optical properties of BiSeI crystal*, Physica status solidi. B, Basic solid state physics. ISSN 0370-1972. Vol. 246, no. 7 (2009), p. 1702-1708.

S5. A. Audzijonis, R. Sereika, R. Žaltauskas, L. Žigas, *Optical spectra of bismuth sulfochloride crystals*, Physica status solidi. B, Basic solid state physics. ISSN 0370-1972. Vol. 247, no. 1 (2010), p. 176-181.

S6. A. Audzijonis, R. Žaltauskas, R. Sereika, L. Žigas, A. Rėza, *Electronic structure and optical properties of BiSI crystal*, Journal of physics and chemistry of solids. ISSN 0022-3697. Vol. 71, iss. 6 (2010), p. 884-891.

S7. A. Audzijonis, R. Sereika, *The thermodynamic functions of SbSBr crystal*, Phase transitions: a multinational journal. ISSN 0141-1594. Vol. 83, iss. 5 (2010), p. 389-395.

S8. A. Audzijonis, L. Žigas, G. Gaigalas, R. Sereika, B. Žygaitienė, *Density functional calculation of the photoelectron emission spectra of BiSCl crystal and molecular clusters*, Journal of cluster science. ISSN 1040-7278. Vol. 21, no. 4 (2010), p. 1-13.

S9. A. Audzijonis, L. Žigas, A. Kvedaravičius, R. Sereika, R. Žaltauskas, A. Čerškus, *Investigation of vibration spectrum ferroelectric semiconductor SbSBr nanowire*, Physica B: Condensed Matter. ISSN 0921-4526. Vol. 405, iss. 17 (2010), p. 3599-3604.

S10. A. Audzijonis, R. Sereika, L. Žigas, R. Žaltauskas, A. Kvedaravičius, *Lattice dynamics of ferroelectric SbSBr crystal*, Ferroelectrics. ISSN 0015-0193. Vol. 413, iss. 1 (2011). p. 434-442.

S11. A. Audzijonis, L. Žigas, R. Sereika, A. Kvedaravičius, *The nature of the ferroelectric phase transition in the modified SbSI ceramics*, Ferroelectrics. ISSN 0015-0193. Vol. 425, iss. 1 (2011), p. 45-53.

S12. A. Audzijonis, R. Sereika, R. Žaltauskas, A. Rėza, *Optical properties of BiSBr and BiSeBr crystals*, Journal of Physics and Chemistry of Solids, ISSN 0022-3697. Vol. 72, iss. 12 (2011), p. 1501-1505.

S13. A. Audzijonis, R. Sereika, R. Žaltauskas, *Birefringence and refractive indices of ferroelectric SbSI*, Phase transitions: a multinational journal. ISSN 0141-1594. Vol. 85, iss. 6 (2012), p. 542-552.

Scientific publications not included in the dissertation

S14. P. Pipinys, A. Audzijonis, R. Sereika, R. Žaltauskas, V. Lapeika, *Current Mechanism in $SbS_{1-x}Se_xI$ Crystals*, Ferroelectrics. ISSN 0015-0193. Vol. 350 (2007), p. 111-117.

S15. A. Audzijonis, R. Sereika, V. Lapeika, R. Žaltauskas, *Current mechanism in SbSeI crystals based on phonon-assisted tunnelling emission*, Physica status solidi. B, Basic solid state physics. ISSN 0370-1972. Vol. 244, no. 9 (2007), p. 3260-3264.

S16. P. Pipinys, R. Sereika, *Comment on 'Conductivity of single $Mo_6S_{9-x}I_x$ molecular nanowire bundles'*, Nanotechnology. ISSN 0957-4484. Vol. 18, iss. 50 (2007). p. 508001-508002.

S17. A. Audzijonis, G. Gaigalas, L. Žigas, R. Sereika, A. Čerškus, A. Pauliukas, R. Žaltauskas, *Investigation of the Vibrational Spectra of a $SbSI(Sb_2S_3)_{0.15}$ Crystals in Harmonic and Anharmonic Approximations*, Ferroelectrics. ISSN 0015-0193. Vol. 377 (2008), p. 22-35.

S18. P. Pipinys, A. Rimeika, R. Sereika, *Phonon-assisted tunneling theories applied to electronic conduction in nanowires of inorganic compounds*, Physics, chemistry and application of nanostructures: reviews and short notes: proceedings of the international conference on nanomeeting 2009: [May 26-29, 2009, Minsk, Belarus]. ISBN 9789814280358 P. 48-51.

Conference thesis of the author on the topic of the dissertation

T1. A. Audzijonis, G. Gaigalas, L. Žigas, R. Sereika, R. Žaltauskas, A. Rėza, *Optical properties of BiSeI crystals*, Radiation interaction with material and its use in

technologies 2008: international conference: Kaunas, Lithuania 24-27 September: program and materials. ISSN 1822-508X p. 258-262.

T2. A. Audzijonis, G. Gaigalas, R. Sereika, L. Žigas, R. Žaltauskas, *BiSI kristalo struktūra (Electronic structure of the BiSI crystal)*, 38-oji Lietuvos nacionalinė fizikos konferencija: programa ir pranešimų tezės, 2009 m. birželio 8-10 d., Vilnius. ISBN 9789955334477 P. 44.

T3. A. Audzijonis, R. Sereika, R. Žaltauskas, A. Rėza, *Optinės BiSI kristalo savybės (Optical properties of the BiSI crystal)*, 38-oji Lietuvos nacionalinė fizikos konferencija: programa ir pranešimų tezės, 2009 m. birželio 8-10 d., Vilnius. ISBN 9789955334477 P. 244.

T4. R. Sereika, A. Budinavičius, S. Garunkštis, *First principles density functional calculations of electronic structure and optical properties in BiSBr and BiSeBr crystals*, Laisvieji skaitymai 2010: 53rd scientific conference for young students of physics and natural sciences: programme and abstracts [2010 March 24-27, 2010, Vilnius, Lithuania] P. 51-52.

T5. A. Audzijonis, L. Žigas, R. Sereika, R. Žaltauskas, A. Kvedaravičius, *Photoelectron emission spectra of BiSCl crystal and molecular cluster*, Radiation interaction with material and its use in technologies 2010: 3rd international conference: Kaunas, Lithuania 20-23 September : program and materials. ISSN 1822-508X p. 122-124.

T6. R. Sereika, A. Audzijonis, R. Žaltauskas, L. Žigas, *Phonon dispersion of SbSBr crystal*, 3rd Workshop on ab-initio phonon calculations: [Poland], Cracow, 2-4 December, 2010, p. 36.

T7. A. Audzijonis, L. Žigas, R. Žaltauskas, R. Sereika, A. Kvedaravičius, V. Šiaudvytis, *SbSeBr optinių savybių tyrimas (Investigation of the optical properties of SbSeBr)*, 39-oji Lietuvos nacionalinė fizikos konferencija: programa ir pranešimų tezės, 2011 m. spalio 6-8 d., Vilnius. ISBN 9789955634645 P. 40.

Conference thesis not included in the dissertation

T8. A. Audzijonis, C. Klingshirn, L. Žigas, A. Pauliukas, R. Žaltauskas, A. Čerškus, A. Kvedaravičius, R. Sereika, *Investigation of the vibrational spectrum of SbSeI*

crystals, Radiation interaction with material and its use in technologies 2006: International conference, Kaunas, Lithuania, 28-30 September, 2006: program and materials. ISSN 1822-508X. Kaunas. 2006, p. 202-207.

T9. A. Audzijonis, G. Gaigalas, L. Žigas, R. Žaltauskas, A. Pauliukas, A. Čerškus, A. Kvedaravičius, R. Sereika, *Teorinis BiSeI molekulinio klasterio valentinių juostų PES tyrimas*, 37-oji Lietuvos nacionalinė fizikos konferencija: programa ir pranešimų tezės, 2007 m. birželio 11-13 d., Vilnius. ISBN 978-9955-33-030-1. Vilnius: Vilniaus universitetas, 2007, p. 218.

T10. R. Sereika, *Current mechanism in SbSeI crystals based on phonon-assisted tunneling emission*, Laisvieji skaitymai 2007: 50th scientific conference for young students of physics and natural sciences, Vilnius, 13 April, 2007. Vilnius: Vilnius University. Faculty of Physics, 2007, p. 41-42.

T11. R. Sereika, A. Audzijonis, *Electron-phonon interaction in BiSeI and BiSI crystals*, 12th International Conference on Phonon Scattering in Condensed Matter: [Paris, France, July 15-20, 2007]. Paris: Institut des Nanosciences de Paris, 2007, p. 141-142.

T12. A. Audzijonis, G. Gaigalas, L. Žigas, R. Sereika, A. Čerškus, A. Pauliukas, R. Žaltauskas, *Ab initio investigation of the vibrational spectra of a* $SbSI(Sb_2S_3)_{0.15}$ *crystals in harmonic approximation*, 2^{nd} Workshop on ab-initio phonon calculations: [Poland], Cracow, 6-8 December, 2007, p. 62.

T13. R. Sereika, *Elektron-fononinės sąveikos temperatūrinė priklausomybė paraelektriniuose ir feroelektriniuose puslaidininkiuose*, Laisvieji skaitymai 2008: 51-oji mokslinė konferencija, Vilnius, 2008 m. balandžio 4 d. p. 93-95.

SHORT INFORMATION ABOUT THE AUTHOR

Raimundas Sereika was born in Druskininkai on 14 of April, 1983. The first degree obtained in Physics and Computer Science (gained physics teachers qualification), Faculty of Physics and Technology, Vilnius Pedagogical University, 2006. In 2008 – Master of Science in Physics and Astrophysics, Faculty of Physics and Technology, Vilnius Pedagogical University. From 2008 to 2012 a PhD student at Lithuanian University of Educational Sciences (Vilnius Pedagogical University).

From 2005 to 2006 was working as a physics teacher at the Vilnius "Gabijos" gymnasium. From 2006 to 2008 was working as an information technologies teacher at the Vilnius "Versmės" secondary school. At the same time, till 2012 was working as a laboratory assistant at Vilnius Pedagogical University. From 2011 till now as a lecturer in the Department of Physics and Information Technologies, Lithuanian University of Educational Sciences.

REZIUMĖ (IN LITHUANIAN)

Disertacijoje teoriškai ir eksperimentiškai nagrinėjami $A^{V}B^{VI}C^{VII}$ tipo junginiai. Teoriniai tyrimai atlikti naudojantis tankio funkcionalo teorija (DFT) kartu su pilno potencialo tiesinių padidintų plokščių bangų (FP-LAPW) metodu ir apibendrinto gradiento aproksimacija (GGA). Skaičiavimams naudoti Wien2k ir PHONON komp. paketai. Eksperimentiniai tyrimai buvo atliekami naudojantis spektroskopinės elipsometrijos metodais bei matuojant dielektrinės skvarbos (elektrinės talpos) priklausomybes nuo temperatūros. Darbe nagrinėjamas $A^{V}B^{VI}C^{VII}$ tipo junginių tarpatominis cheminis ryšys, elektroninė struktūra, optinės savybės, gardelės dinamika, virpesių termodinaminės funkcijos ir dielektriniai pokyčiai paraelektrinėje, feroelektrinėje ir antiferoelektrinėje fazėse.

Cheminio ryšio tyrimui buvo skaičiuojamas elektronų krūvio tankio pasiskirstymas, įvertinti kovalentinis ir joninis faktoriai. Junginių elektroninė struktūra ir optinės savybės tyrinėtos atlikus tūrinę optimizaciją bei nustačius tinkamiausią tikslinančią aproksimaciją. Apskaičiuoti ir aprašyti elektronų būsenų tankiai, elektroninė juostinė sandara. Apskaičiuotos ir aprašytos optinės dielektrinės, lūžio rodiklių, sugerties rodiklių, elektronų energijos nuostolių, sugerties ir atspindžio koeficientų funkcijos. Apskaičiuotas teorinis SbSI kristalo dvejopas lūžis feroelektrinio fazinio virsmo srityje. Gardelės dinamika tyrinėta skaičiuojant fononų būsenų tankius ir virpesių dispersiją. Apskaičiuota fononų laisvoji energija, šiluminiai poslinkiai, Helmholtzo laisvoji energija, vidinė energija ir entropija. Taip pat apskaičiuoti šių funkcijų skirtumai tarp paraelektrinės ir feroelektrinės fazės. Nustatyta anharmonizmo įtaka termodinaminėms funkcijoms ir fazinio virsmo atsiradimui. Dielektriniai pokyčiai tyrinėti 270-440 K temperatūros srityje. SbSI ir SbSeI kristaluose atrastas dielektrinio spektro maksimumas ~ 410 K temperatūroje. Aprašytos šio maksimumo atsiradimo priežastys ir jį įtakojantys veiksniai.

Teoriniai ir eksperimentiniai rezultatai palyginti tarpusavyje, o taip pat su kitų autorių rezultatais paskelbtais literatūroje. Darbo pabaigoje suformuluotos bendrosios išvados. Pateiktas cituotų literatūros šaltinių sąrašas ir priedas su papildomais, darbe naudotais duomenimis teoriniams skaičiavimams.